Dear Dr. Andreas Hofzumahaus,

We have considered all of the comments from the two reviews and, in most cases, revised the manuscript to address them. A detailed response for each comment is listed below.

As a result, the manuscript has been significantly strengthened and we very much appreciate your consideration for publication in Atmospheric Measurement Techniques.

Sincerely,
Andrew Thorpe and coauthors

Response to reviewer comments

Anonymous Referee #1 comments:

In their paper on airborne DOAS retrievals Andrew K. Thorpe et al. demonstrate that small-scale plumes of greenhouse gases can be detected with their measurement system. Based on established retrieval theory they present an application where the mutual interference of spectral signatures is addressed by jointly fitting the concentrations of the related species. They demonstrate the capability of their method in a predictivist sense, i.e. they compare their retrieved data to use-novel data (data which have not been used in the retrieval as e.g. a priori information) to confirm their results. This approach is valid and apt to furnish evidence that the method chosen is indeed adequate and has the claimed merits. Further, the paper is well written and clearly structured, and there seems not much to be criticized.

However, I think, the paper still could be improved. Modern retrieval theory offers a lot of diagnostics which would be interesting in the given context: averaging kernels (spatial resolution and content of prior information in the data), retrieval covariance matrices (particularly retrieval error bars and detection limits inferred from these), etc. A thorough discussion of these quantities would probably shift the focus of the paper. Since a reviewer should not dictate the authors the focus of their paper, and since their way to demonstrate the capability of their measurement system and retrieval method is already convincing, I am reluctant to force the authors to include the discussion of these quantitative diagnostic data and only encourage them to consider this issue if they can easily accommodate it. At least typical retrieval errors should be easy to include. In summary, I recommend publication of this paper in AMT after correction of the following technical issues:

Response: We thank the reviewer for their thorough and helpful comments. We agree with the assessment that a detailed sensitivity study is outside the scope of the paper and would significantly shift the focus of the study. However, these are very relevant topics that merit further discussion. In the context of this manuscript, a discussion of typical retrieval errors was included (see page 10, line 16 to page 11, line 24).

p7 l8: I there a version number of this particular HITRAN data set available?

Response: The 2008 version has been explicitly specified in the text (see page 8, line 16). This is consistent with the reference (Rothman et al., 2009).

p8 l2: ...these Jacobians are not shown. ("in Figure 1" can be deleted because it is clear from the context).

Response: This is a good point, “in Figure 1” is redundant and was removed (see page 8, line 11).

p8 l18/19 (attention: line numbering is not monotonic in my version here and on the following pages!) It is reported which gases are "included" in which retrieval. This is, however, ambiguous. This can mean "included in the forward calculation of the retrievals, using their respective a priori profiles and leaving these as they are" or it can mean "included as additional unknown variables of the retrieval". I guess you mean the latter but you should be more specific here.

Response: The language has been clarified by using the term “as additional unknown variables of the retrieval” (see page 8, line 12).

p10 l7 "An H2O retrieval..."; (replace "A" by "An")

Response: The typo was corrected here (see page 12, line 19) and throughout the rest of the manuscript.

p11 l14 "spectral mixing": Is this an established technical term in your community? In my community the superposition of spectral signatures from various species is typically called "spectral interference" or we use phrases like "signal from interfering species".

Response: Spectral interference is indeed a better choice. This change has been made in the main body of the manuscript (see page 13, line 23; page 15, line 11) and abstract.

p13 l32 knowN

Response: This typo was corrected (see page 15, line 8).

p14 l6 Appendix A is printed twice.

Response: The extra “Appendix A” text has been removed (see page 16).

Anonymous Referee #2 comments:

General comments

In the paper, the authors apply IMAP-DOAS algorithm to the AVIRIS-NG instrument for mapping CO2, CH4 and H2O plumes for seven sources. The topic of the paper is well within the scope of AMT. The methods are valid and the authors present new data. However, some results are not sufficient to support some interpretation and conclusions in the paper. The paper lacks a description and discussion of measurement uncertainties making it very difficult to evaluate the quality of the results.

The authors repeatedly state that they identified over 250 CH4 plumes with AVIRIS-NG, but they only show four examples where IMAP-DOAS was applied. They authors need to explain the reasons for choosing these four plumes and for omitting the others. Furthermore, the advantage of IMAP-DOAS over the matched filter is not clearly stated giving the impression that IMAP-DOAS is actually inferior to the filter because only four plumes are detectable.

Response: Thank you for this observation, we can understand that this could generate some confusion. We have added additional text to explain the linearized matched filter, how it differs from the IMAP-DOAS approach, and the rationale for why IMAP-DOAS results were generated for a subset of the plumes identified in a previous study (Frankenberg et al., 2016). Please refer to the first two paragraphs of section 5.1 (page 11).

To conclude, the authors should describe measurement uncertainties and discuss how IMAP-DOAS compares to and differs from the linearized matched filter approach.

Response: Reviewer 2 brings up this point which was also discussed by Reviewer 1. A detailed uncertainty analysis between IMAP-DOAS and the linearized matched filter is beyond the scope of this paper. However, a discussion of typical IMAP-DOAS retrieval errors is appropriate and was included (see page 10, line 16 to page 11, line 24).

The authors claim that they are able to detect H2O from cooling towers (Figure A4d). However, I am not able to identify these plumes in Figure A4d. The figure shows a large area of enhanced scaling factors east of the cooling ponds, but this H2O signal more likely originates from the ponds. I agree that wind directions at cooling towers and stacks can be different due to temporal variability or the height dependency of the wind direction (Ekman spiral). However, since the plumes a very short and likely meandering, it is very difficult to estimate the wind direction from the true color composite alone in Figure A5a. Nonetheless, I think the wind direction at the cooling tower is more southerly than indicated by the blue arrows. To conclude, the authors need to add more support for their claim that H2O has been detected from the cooling towers.

Response: This is a very astute observation and the authors agree that the observed H2O signal could be a combination of both H2O from the cooling towers in addition to the cooling ponds. This distinction was made on page 14, line 35-36 as well as in the abstract.

In summary, I recommend publication of this paper in AMT after adding the points above as well as the following specific comments and technical corrections.

Response: We appreciate the reviewer's detailed assessment of this work and constructive comments.

Specific comments

• Adding a map showing all measurements sites to the paper would make it easier to locate the sites.

Response: We agree with the reviewer and have added a new figure showing the locations of the sites (see page 4, Figure 2).

• The authors should change their units from ppm m to a more common unit such as dry air column averaged mole fractions (XCO2 and XCH4).

Response: We determined that it would be best to use a colorscale showing units in both ppm-m and the gas state vector at the last iteration of the retrieval (gas scaling factor). This ensures consistency with a number of previous studies (Thorpe et al., 2014, 2016; Thompson et al., 2015, 2016; Frankenberg et al., 2016).

Technical corrections

• Page 6, Section 5.1, 3rd paragraph: Add full stop after “east edge of the AVIRISNG scene”

Response: This typo was corrected (see page 11, line 15).

• Page 7, line 39: Frankenberg et al. (2016) -> (Frankenberg et al. 2016)

Response: We could not find this at the stated location (page 7, line 39), but we believe the reviewer was referring to page 12, line 29-30, where the correction was made two times.

Airborne DOAS retrievals of methane, carbon dioxide, and water vapor concentrations at high spatial resolution: application to AVIRIS-NG

Andrew K. Thorpe [1], Christian Frankenberg [2,1], David R. Thompson [1], Riley M. Duren [1], Andrew D. Aubrey [1], Brian D. Bue [1], Robert O. Green [1], Konstantin Gerilowski [3], Thomas Krings [3], Jakob Borchardt [3], Eric A. Kort [4], Colm Sweeney [5], Stephen Conley [6,7], Dar A. Roberts [8], and Philip E. Dennison [9]

[1]Jet Propulsion Laboratory, California Institute of Technology, Pasadena, California, United States
[2]California Institute of Technology, Pasadena, California, United States
[3]Institute of Environmental Physics (IUP), University of Bremen, Bremen, Germany
[4]University of Michigan, Ann Arbor, United States
[5]Cooperative Institute for Research in Environmental Sciences, University of Colorado, Boulder, CO, United States
[6]Global Monitoring Division, NOAA Earth System Research Laboratory, Boulder, Colorado, United States
[7]Scientific Aviation, 3335 Airport Road, Boulder, Colorado, United States
[8]University of California, Santa Barbara, Santa Barbara, California, United States
[9]University of Utah, Salt Lake City, Utah, United States

Correspondence to: Andrew K. Thorpe (Andrew.K.Thorpe@jpl.nasa.gov)

Abstract. At local scales, emissions of methane and carbon dioxide are highly uncertain. Localized sources of both trace gases can create strong local gradients in its columnar abundance, which can be discerned using absorption spectroscopy at high spatial resolution. In a previous study, more than 250 methane plumes were observed in the San Juan Basin near Four Corners during April 2015 using the next generation Airborne Visible/Infrared Imaging Spectrometer (AVIRIS-NG) and a linearized matched filter. For the first time, we apply the Iterative Maximum a Posteriori Differential Optical Absorption Spectroscopy (IMAP-DOAS) method to AVIRIS-NG data and generate gas concentration maps for methane, carbon dioxide, and water vapor plumes. This demonstrates a comprehensive greenhouse gas monitoring capability that targets methane and carbon dioxide, the two dominant anthropogenic climate-forcing agents. Water vapor results indicate the ability of these retrievals to distinguish between methane and water vapor despite spectral interference in the short wave infrared. We focus on selected cases from anthropogenic and natural sources, including emissions from mine ventilation shafts, a gas processing plant, tank, pipeline leak, and natural seep. In addition, carbon dioxide emissions were mapped from the flue-gas stacks of two coal-fired power plants and a water vapor plume was observed from the combined sources of cooling towers and cooling ponds. Observed plumes were consistent with known and suspected emission sources verified by the true color AVIRIS-NG scenes and higher resolution Google Earth imagery. Real time detection and geolocation of methane plumes by AVIRIS-NG provided unambiguous identification of individual emission source locations and communication to a ground team for rapid follow up. This permitted verification of a number of methane emission sources using a thermal camera, including a tank and buried natural gas pipeline.

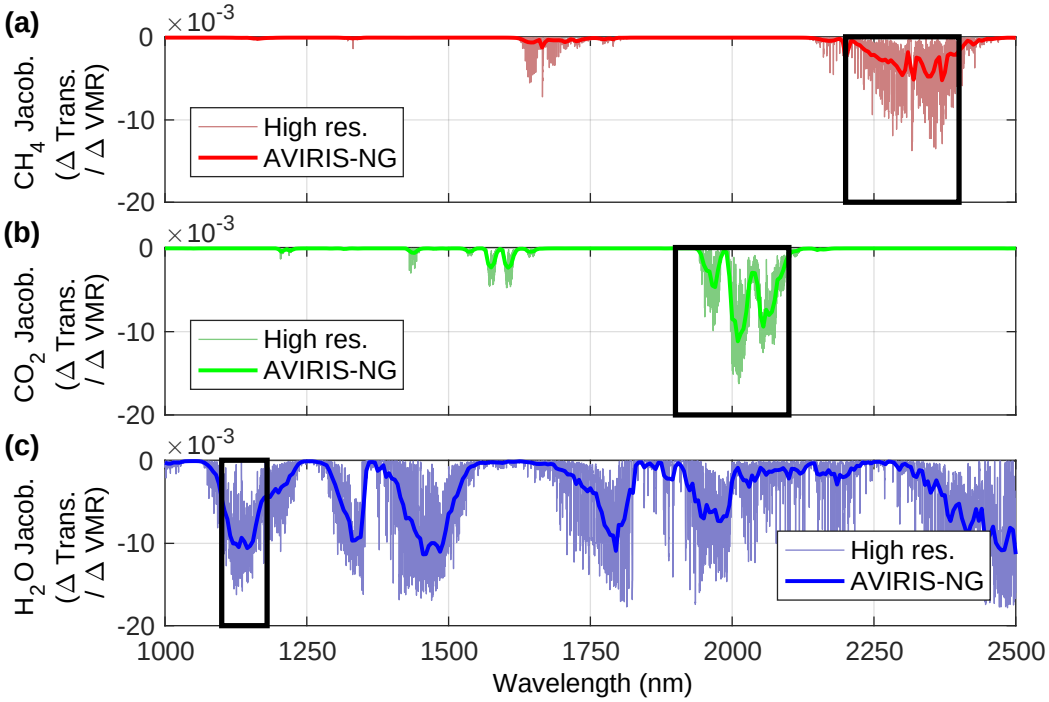

Figure 1. High resolution gas Jacobians plotted in lighter colors and for AVIRIS-NG (5 nm spectral resolution and sampling) for (a) CH_4 (red), (b) CO_2 (green), and (c) H_2O (blue). These examples were calculated for a 5 % change in CH_4 (red), (b) CO_2 (green), and (c) H_2O over the total column. AVIRIS-NG retrieval windows are indicated by the black outlines.

1 Introduction

It is important to better understand the processes controlling changes in atmospheric methane (CH_4) and carbon dioxide (CO_2), the two dominant anthropogenic climate-forcing agents. CH_4 and CO_2 contribute approximately 17 % and 64 % of the total radiative forcing attributed to anthropogenic greenhouse gases and halocarbons (Myhre et al., 2013). The atmospheric growth rates are strongly influenced by anthropogenic emissions of CH_4 and dominated by fossil fuel CO_2 emissions. Anthropogenic CH_4 sources were estimated to contribute 10.6 % of the total 2014 anthropogenic emissions of the United States, with major sources including natural gas systems (2.6 %), enteric fermentation (2.4 %), landfills (2.2 %), petroleum systems (1.0 %), coal mining (1.0 %) (EPA, 2016a). CH_4 is a precursor for tropospheric ozone and is strongly linked with co-emitted reactive trace gases that are the focus of air quality mitigation policies. U.S. anthropogenic CO_2 sources make up 81 % of the total anthropogenic emissions and are dominated by fossil fuel combustion, including electricity generation (30 %), transportation (25 %), and industrial emissions (12 %) (EPA, 2016a). U.S. emissions of both gases are projected to increase (EIA, 2013) and a number of studies have suggested that EPA bottom up emission inventories are underestimated for CH_4 (Miller et al., 2013; Wecht et al., 2014; Turner et al., 2015). U.S. fossil fuel CO_2 emissions are better constrained through existing inventories of fossil

fuel sales and combustion, however, global uncertainties are growing with the rise of a number of large, developing countries where emissions information is not readily available (NRC, 2010; Ballantyne et al., 2015; Ciais et al., 2015).

There remains uncertainty regarding the sources and sinks of atmospheric CH_4, as reflected by the ongoing scientific discussion on both the hiatus in the atmospheric growth rate in the early 21st century as well as the unexpected rise starting in 2007 (Nisbet et al., 2014). Further, regional top-down emissions estimates cannot discriminate source categories and thereby attribute fluxes to specific processes or sources. Uncertainty in anthropogenic CH_4 emissions is large at multiple scales and process attribution remains challenging because emissions originate from biological processes, venting, and leaks (Kirschke et al., 2013; Schwietzke et al., 2016; Schaefer et al., 2016).

Recent studies suggest that the majority of CH_4 emissions from oil and gas supply chains are caused by a number of super-emitters, which could explain underestimates in bottom-up inventories (Zavala-Araiza et al., 2015; Lyon et al., 2015; Brandt et al., 2014, 2016). The ability to identify emission sources offers the potential to constrain regional greenhouse gas budgets and improve partitioning between anthropogenic and natural emission sources. Although CH_4 has a short atmospheric lifetime (about 9 years), it has a very high Global Warming Potential (GWP) which is 86 times greater than CO_2 on a 20 year time scale (Myhre et al., 2013). This means that even small amounts of emissions reduction will result in large reductions in the overall atmospheric radiative forcing.

Driving surveys using in situ instruments have been used to identify CH_4 emission sources in major U.S. metropolitan areas like the Los Angeles basin (Hopkins et al., 2016), Boston (Phillips et al., 2013), and Washington, D.C. (Jackson et al., 2014) as well as to measure fluxes (Rella et al., 2015). Recently, ground-based thermal imaging systems have also been used to identify CH_4 emissions (Johnson et al., 2015; Galfalk et al., 2016). However, these methods require comprehensive sampling techniques, are time consuming, and can be limited to regions with sufficient road access. In situ airborne measurements offer the potential for increased coverage and have been used for U.S. regional CH_4 flux estimates using mass balance approaches for the Uintah Basin in northeastern Utah (Karion et al., 2013), the Marcellus formation in southwestern Pennsylvania (Caulton et al., 2014), and the Barnett Shale formation in Texas (Smith et al., 2015; Lavoie et al., 2015). These measurements reflect gas concentrations at the flight altitude and these studies are designed to estimate aggregate emissions for large regions rather than identifying individual emissions sources.

More recently, in situ airborne measurements using a chemically-instrumented Mooney aircraft have been used to estimate fluxes from known sources like the Aliso Canyon leak (Conley et al., 2016) and for a number of sources identified by imaging spectrometers in the Four Corners region (Frankenberg et al., 2016). This method samples the atmosphere directly at the flight path altitude and can measure multiple gas species. The Methane Airborne MAPper (MAMAP) spectrometer (Gerilowski et al., 2011) has also been used to measure elevated CH_4 and CO_2 column abundances to quantify emissions from a coal mine ventilation shaft (Krings et al., 2013), power plants (Krings et al., 2011), and a landfill (Krautwurst et al., 2016). MAMAP is a non-imaging spectrometer with a small field of view limited to flying transects across gas plumes rather than quickly mapping their morphology and extent on small scales. Both instruments are better suited for investigating either known emission sources or identifying larger regional emissions as opposed to individual sources.

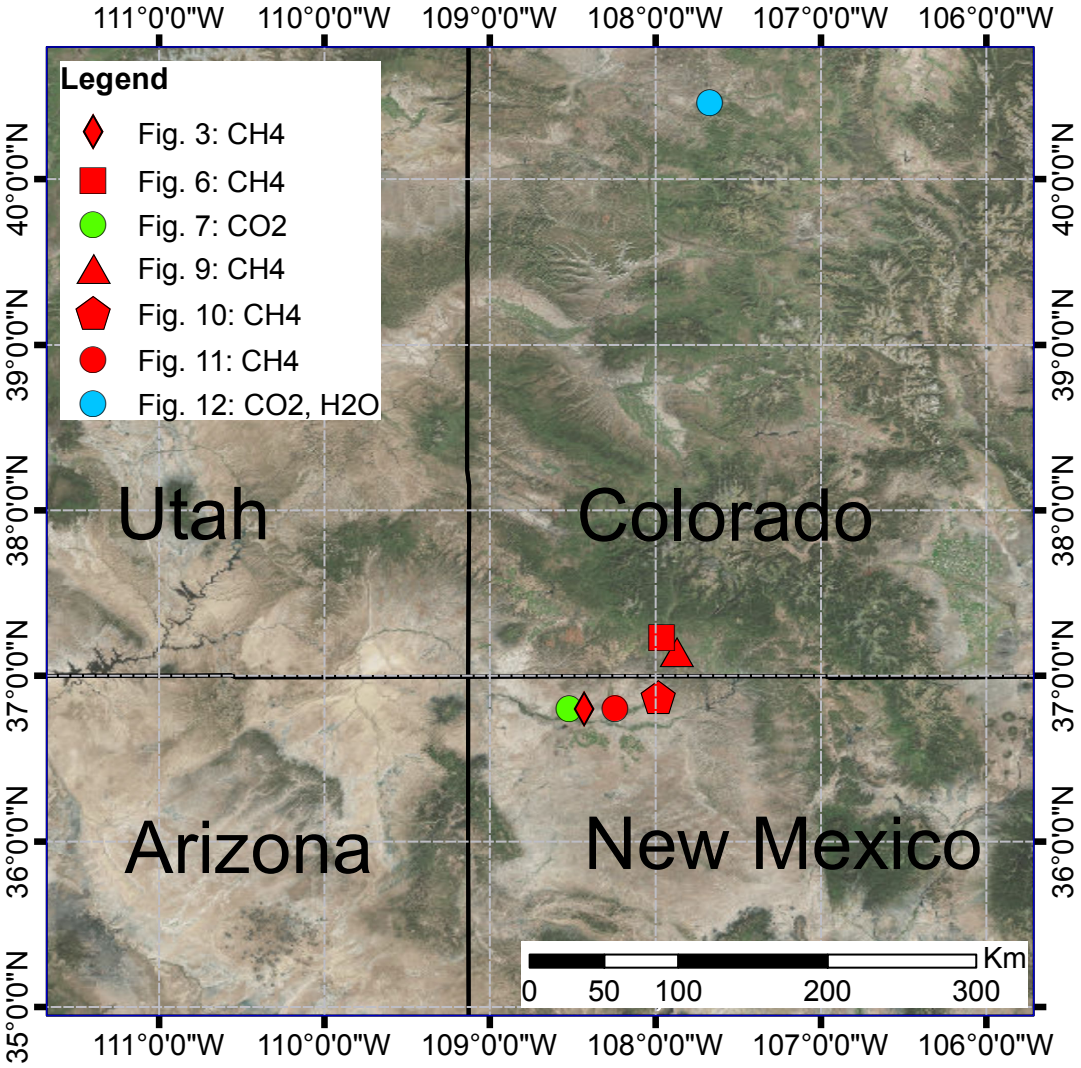

Figure 2. Locations of gas plumes presented in this study.

2 Airborne imaging spectrometers

Airborne imaging spectrometers like the Airborne Visible/Infrared Imaging Spectrometer (AVIRIS) (Green et al., 1998) and the next generation instrument AVIRIS-NG (Hamlin et al., 2011) can map large regions while providing the spatial resolution required to identify individual emissions within scenes. While not originally designed for mapping emissions, these instruments measure the 0.38 to 2.5 μm range that includes many gas absorption features (Figure 1). This has permitted quantitative retrievals of CH_4 using AVIRIS (approximately 10 nm spectral resolution and sampling) for marine seeps (Roberts et al.,

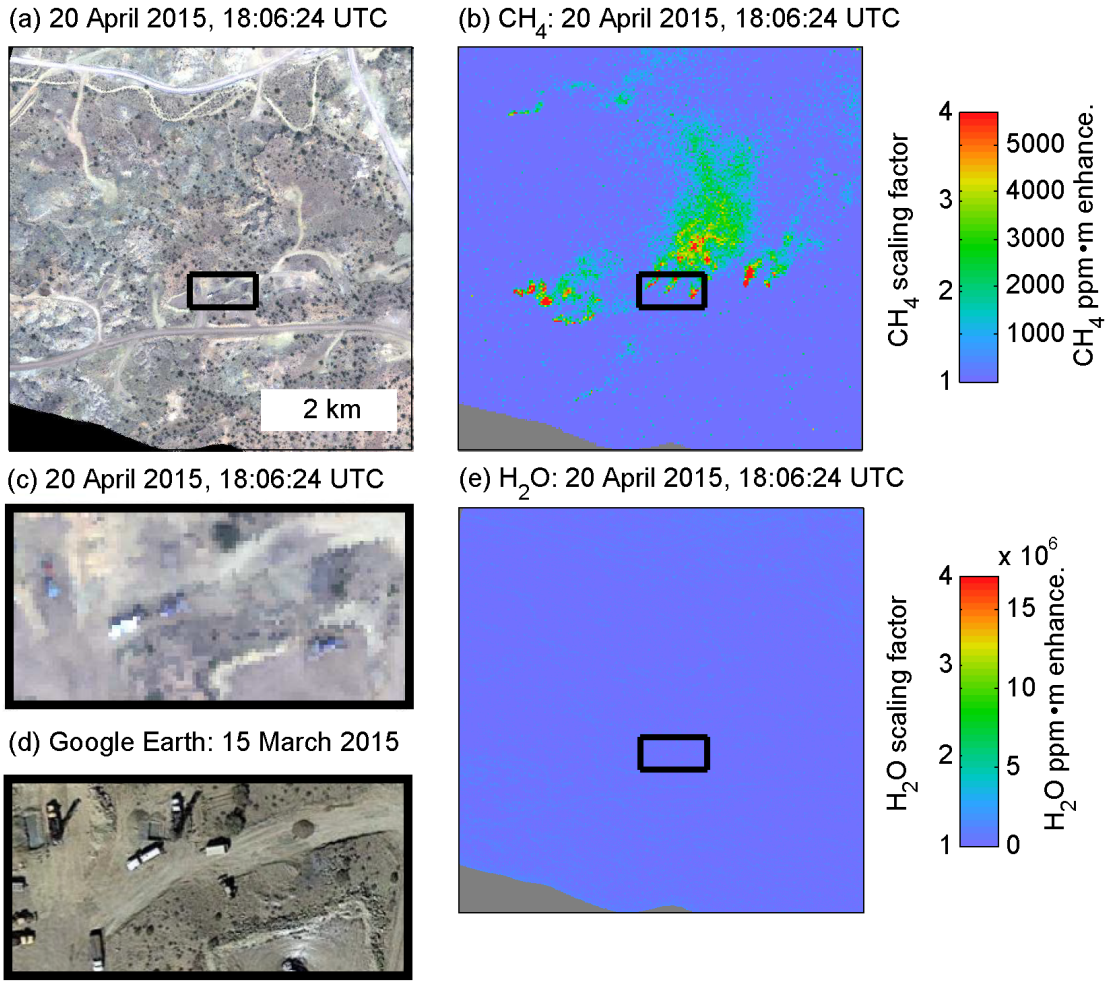

Figure 3. (a) AVIRIS-NG true color image subset. (b) A number of CH_4 plumes are clearly visible with maximum enhancements in excess of 5,000 ppm•m. (c) Close up of AVIRIS-NG true color image shown by black outline in (a). (d) Higher resolution Google Earth imagery for same area reveals drilling rigs at an active underground coal mine, suggesting the origin of these plumes are mine workings ventilation shafts. (e) H_2O retrieval does not indicate enhancements. For all images, north is up.

2010; Thorpe et al., 2014). Water vapor retrievals have been demonstrated with AVIRIS (Gao and Goetz, 1990; Thompson et al., 2015a) mainly for atmospheric correction and reflectance retrievals. However, AVIRIS water vapor retrievals have also been used to measure plant transpiration, demonstrating potential application to the fields of ecology and meteorology (Ogunjemiyo et al., 2004).

AVIRIS has been used for high resolution mapping of CO_2 plumes from industrial sources (Dennison et al., 2013) and wildfires (Marion et al., 2004; Deschamps et al., 2011). More recently, AVIRIS-NG (approximately 5 nm spectral resolution

and sampling) has surveyed large regions to identify CH_4 emissions associated with oil production (Thompson et al., 2015b), gas extraction (Frankenberg et al., 2016), hydraulic fracturing (Aubrey et al., 2015), and a landfill (Krautwurst et al., 2016). This is possible due to a 34° field of view, which results in an image swath of 1.8 km when flying at 3 km above ground level (AGL).

Airborne imaging spectrometers that operate in the thermal infrared, such as the Mako and HyTES instruments (Tratt et al., 2014; Hulley et al., 2016), have also been used for mapping CH_4 plumes. However, the altitude of maximum sensitivity varies with environmental conditions like thermal contrast (Kuai et al., 2016), which can make plumes difficult to detect and quantify, and sensitivity to near surface emissions decreases with flight altitude, which can limit ground coverage. Because AVIRIS and AVIRIS-NG measure reflected solar radiation in the short wave infrared, CH_4 retrieval sensitivity is impacted only slightly by flight altitude due to additional gas attenuation along the optical path. However, at higher flight altitude and coarser spatial resolution a gas enhancement is diluted over a larger image pixel, thereby decreasing instrument sensitivity. The ability to fly high results in more efficient flight campaigns due to improved ground coverage. For example, AVIRIS-NG consistently observed plumes for a CH_4 controlled release experiment for all altitudes flown (up to 3.8 km AGL) and AVIRIS has observed CH_4 plumes flying at 8.9 km AGL (Thorpe et al., 2014). AVIRIS has also mapped CH_4 plumes over multiple days from the Aliso Canyon leak by flying 6.6 km AGL, resulting in an image swath approximately 4.0 km wide (Thompson et al., 2016). This also offers the potential for space-based detection of emission sources, like the observed CH_4 plume from Aliso Canyon using the orbital Hyperion imaging spectrometer (Thompson et al., 2016).

In a previous study (Thorpe et al., 2014), the Iterative Maximum a Posteriori Differential Optical Absorption Spectroscopy (IMAP-DOAS) retrieval was applied to AVIRIS for quantitative mapping of CH_4 from natural and anthropogenic sources. In this study, the application of IMAP-DOAS has been expanded for use with AVIRIS-NG for multiple gas species, including CH_4, CO_2, and H_2O. We present results from AVIRIS-NG data acquired in New Mexico and Colorado, including from a flight campaign in the San Juan Basin near Four Corners. We will present results for a number of sources, including CH_4 from mine ventilation shafts, a gas processing plant, tank, pipeline leak, and natural seep, as well as CO_2 and H_2O plumes associated with power plants (Figure 2).

3 Study sites and AVIRIS-NG data

Space-based observations collected by the SCanning Imaging Absorption SpectroMeter for Atmospheric CHartographY (SCIAMACHY) instument (Bovensmann et al., 1999) showed CH_4 enhancements in the Four Corners region (Kort et al., 2014). This made for an ideal location for follow up surveys using AVIRIS-NG to identify individual emission sources. During the flight campaign, the AVIRIS-NG instrument was equipped with a real time CH_4 mapping capability using a waterfall display monitored by the instrument operator. Observed CH_4 plumes were overlaid on a true color image displaying location information as well as the maximum CH_4 enhancement (Thompson et al., 2015b). This permitted adaptive survey strategies to investigate observed plumes and the ability to send images of the plume with accurate locations to a ground crew for subsequent follow

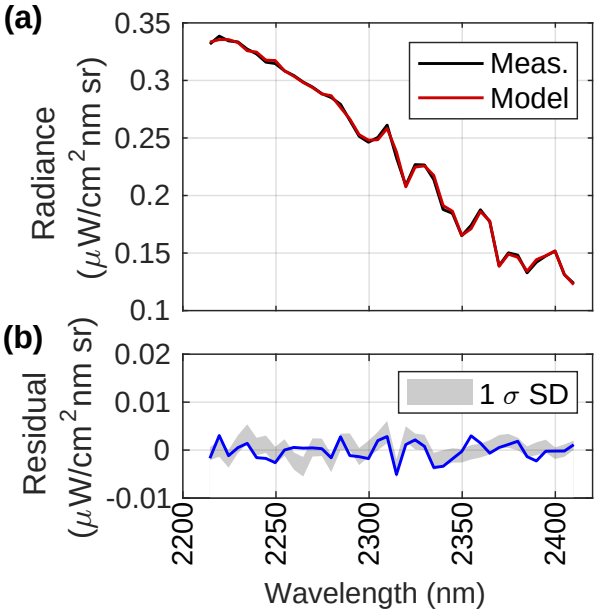

Figure 4. (a) AVIRIS-NG measured and modeled radiance for one image pixel within the CH_4 plume used for the CH_4 retrieval (see Figure 3b). (b) The residual is plotted with 1 σ standard deviation boundary calculated from residuals for the entire scene.

up. A Xenics Onca-VLWIR-MCT-384 thermal imaging camera with a Spectrogon optical filter centered at 7.746 μm was used by the ground crew to verify a number of plumes observed in real time by AVIRIS-NG.

Located in New Mexico and Colorado, the San Juan Basin produces natural gas from sandstone, coal bed CH_4, and shale formations and is the fourth largest U.S. gas field when it comes to total production (EIA, 2015). During a five day campaign in April 2015, AVIRIS-NG targeted an area corresponding to the highest CH_4 enhancements observed with SCIAMACHY (Frankenberg et al., 2016). A 2,500 km^2 area was covered in approximately two days (9.2 flight hours) flying at 3 km above ground level, resulting in scenes with an image swath of around 1.8 km and a ground resolution of 3 m. The remaining flight days were used for additional follow up flights and some repeat observations, sometimes at lower flight altitudes. During the campaign, a number of potential CH_4 emission sources were targeted, including infrastructure associated with natural gas production like wellpads, tanks, and gas processing plants, a coal mine, and natural coal bed CH_4 seeps. While the flight campaign focused on CH_4 sources, the coal-fired San Juan power generating station was also flown as a potential CO_2 emission source.

4 IMAP-DOAS retrievals

A detailed description of the IMAP-DOAS retrieval for AVIRIS can be found in Thorpe et al. (2014). Gas retrievals were performed on orthocorrected radiance data. Atmospheric profiles were generated by updating prior gas profiles from the U.S.

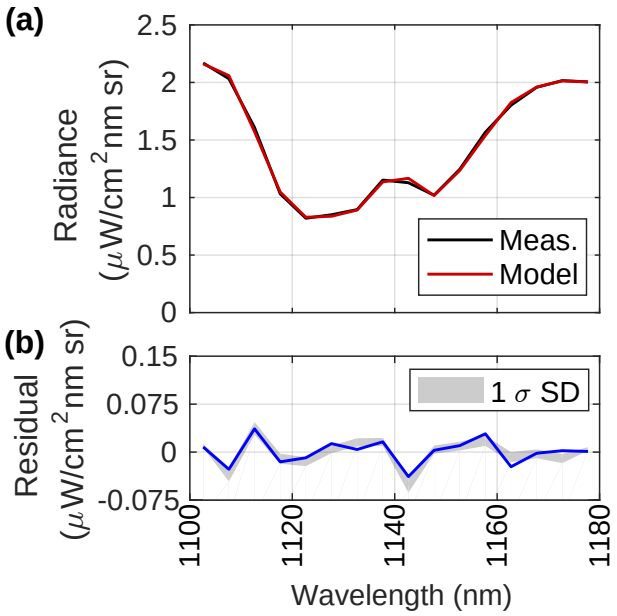

Figure 5. (a) AVIRIS-NG measured and modeled radiance for one image pixel within the CH_4 plume used for the H_2O retrieval (see Figure 3e). (b) The residual is plotted with 1 $\boldsymbol{\sigma}$ standard deviation boundary calculated from residuals for the entire scene.

standard atmosphere obtained from the radiative transfer models LOWTRAN/MODTRAN (Kneizys et al., 1996) using volume mixing ratios (VMR) from the NOAA Mauna Loa station, United States (NOAA, 2015). Temperature, pressure, and water vapor VMR profiles representative of the time period of the flight campaign were acquired from the National Centers for Environmental Prediction/National Center for Atmospheric Research (NCEP/NCAR) Reanalysis project (Kalnay et al., 1996). Spectral parameters for CH_4, CO_2, H_2O, and N_2O were used from the HITRAN 2008 database (Rothman et al., 2009) and a classical Voigt spectral line-shape was used to calculate vertical optical densities for fourteen atmospheric layers that spanned sea level to the top of the atmosphere.

Above the aircraft, vertical optical densities were combined and an air mass factor (AMF) was calculated to account for one way transmission. Vertical optical densities below the aircraft were also combined with an AMF reflecting two way transmission. This resulted in a two layer atmospheric model that speeds up the retrieval and incorporates the ground elevation and flight altitude for each AVIRIS-NG scene. The two layer model was used to model reflected solar radiation perturbed by the absorbing species CH_4, CO_2, H_2O, and N_2O. Three retrieval windows were used, each targeting the primary gas of interest. CH_4 retrievals were performed between 2,215 and 2,410 nm (Figure 1) and included fits for H_2O and N_2O. Gas Jacobians that reflect changes in absorption due to the absorbing species CH_4, CO_2, H_2O are shown in Figure 1. Because N_2O has weak absorption features, these Jacobians are not shown. Between 1,904 and 2,099 nm, CO_2 retrievals included H_2O and N_2O as additional unknown variables of the retrieval, while H_2O retrievals between 1,103 and 1,178 nm also included CO_2 and N_2O. Therefore, the state vector ($\boldsymbol{x}_n$) for each retrieval window has 6 entries (three gases for two atmospheric layers).

Modeled radiance at high spectral resolution was calculated for each wavelength with a forward radiative transfer model using the following equation

$$\boldsymbol{F}^{\mathrm{hr}}(\boldsymbol{x}_i) = \boldsymbol{I}_0^{\mathrm{hr}} \cdot \exp\left(-\sum_{n=1}^{6} \boldsymbol{A}_n \cdot \boldsymbol{\tau}_n^{\mathrm{ref}} \cdot \boldsymbol{x}_{n,i}\right) \cdot \sum_{i=0}^{k} a_k \lambda^k \tag{1}$$

where $\boldsymbol{F}^{\mathrm{hr}}(\boldsymbol{x}_i)$ is the forward modeled radiance at the ith iteration of the state vector, $\boldsymbol{I}_0^{\mathrm{hr}}$ is the incident intensity, a solar transmission spectrum (Geoffrey Toon, personal communication, 2013), $\boldsymbol{A}_n$ is the air mass factor (AMF) for each n number of atmospheric state vector elements, $\boldsymbol{\tau}_n^{\mathrm{ref}}$ is the reference vertical optical density for each n number of atmospheric state vector elements (including optical densities of the three absorbing species, $\boldsymbol{x}_{n,i}$ is the trace gas related state vector at the ith iteration, which scales the prior optical densities of each of the absorbing species in each n layer (six rows, three gases for two atmospheric layers), a_k are polynomial coefficients to account for low-frequency spectral variations.

The state vector contains the spectral shift (not shown here) and a low order polynomial function (a_k) to account for the broadband variability in surface albedo (see Frankenberg et al. (2005). The high resolution modeled radiance is convolved using the the instrument line shape function and sampled to the center wavelengths for each AVIRIS-NG spectral band, resulting in a lower resolution modeled radiance at the ith iteration of the state vector $\boldsymbol{F}^{\mathrm{lr}}(\boldsymbol{x}_i)$, calculated using a known $\boldsymbol{\tau}_n^{\mathrm{ref}}$ scaled by $\boldsymbol{x}_{n,i}$.

A Jacobian Matrix is calculated for each iteration i, where each column represents the derivate vector of the sensor radiance with respect to each element of the state vector ($\boldsymbol{x}_i$).

$$\mathbf{K}_i = \left.\frac{\partial \boldsymbol{F}^{\mathrm{lr}}(\boldsymbol{x})}{\partial \boldsymbol{x}}\right|_{\boldsymbol{x}_i}. \tag{2}$$

The state vector at the ith iteration can be optimized as follows (Rodgers, 2000)

$$\begin{aligned}\boldsymbol{x}_{i+1} = \boldsymbol{x}_{\mathrm{a}} + \left(\mathbf{K}_i^T \mathbf{S}_\varepsilon^{-1} \mathbf{K}_i + \mathbf{S}_{\mathrm{a}}^{-1}\right)^{-1} \mathbf{K}_i^T \mathbf{S}_\varepsilon^{-1} \\ \cdot \left[\boldsymbol{y} - \boldsymbol{F}^{\mathrm{lr}}(\boldsymbol{x}_i) + \mathbf{K}_i(\boldsymbol{x}_i - \boldsymbol{x}_{\mathrm{a}})\right]\end{aligned} \tag{3}$$

where $\boldsymbol{x}_{\mathrm{a}}$ is the a priori state vector (six rows), $\boldsymbol{x}_i$ is the state vector at the ith iteration (six rows), $\mathbf{S}_\varepsilon$ is the error covariance matrix, $\mathbf{S}_{\mathrm{a}}$ is the a priori covariance matrix, $\boldsymbol{y}$ is the measured AVIRIS-NG radiance, $\boldsymbol{F}^{\mathrm{lr}}(\boldsymbol{x}_i)$ is the forward model evaluated at $\boldsymbol{x}_i$, and $\mathbf{K}_i$ is the Jacobian of the forward model at $\boldsymbol{x}_i$.

The retrieval optimizes a scaling factor relative to the a priori profile. The a priori scaling factor is set to one as an initial guess for each gas in the two layers, while the a priori covariance matrix was set to constrain the fit to the atmospheric layer beneath the aircraft where high variance is expected. To do so, very small prior covariances were set for the uppermost layer (above the aircraft). Because the observed plumes are not expected to extend above the AVIRIS-NG flight altitude, this assumption is reasonable. Gas concentrations were calculated in ppm·m by multiplying the gas state vector at the last iteration (gas scaling factor) by the VMR for the lowest layer of the reference atmosphere and the distance between the aircraft and the ground. In subsequent figures, color bars will indicate the scaling factors as well as gas enhancements relative to background, which were calculated by subtracting the retrieved gas concentration from the background concentration for the lowest layer of the reference atmosphere.

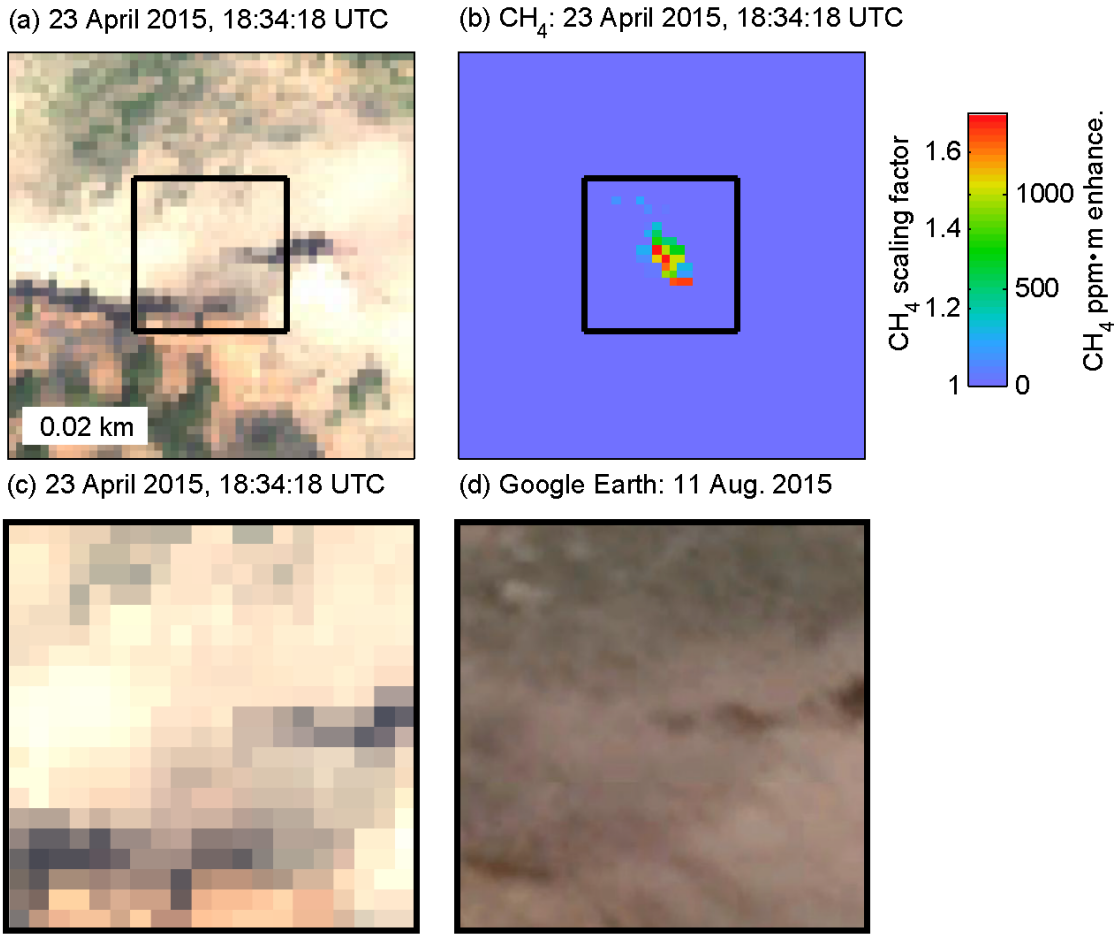

Figure 6. (a) AVIRIS-NG true color image subset. (b) A small CH_4 plume is visible from a confirmed geological source at Moving Mountain near Durango, Colorado. (c) Close up of AVIRIS-NG true color image. (d) Higher resolution Google Earth imagery provides additional spatial context. For all images, north is up.

The covariance $\hat{S}$ was calculated to estimate expected IMAP-DOAS retrieval errors as follows:

$$\hat{S} = \left(\mathbf{K}^T \mathbf{S}_{\varepsilon}^{-1} \mathbf{K} + \mathbf{S}_{\mathrm{a}}^{-1}\right)^{-1} \tag{4}$$

where the diagonal of $\hat{S}$ corresponds to the covariance at each atmospheric layer associated with the gases used for each fitting window. $\mathbf{S}_{\varepsilon}$, the error covariance matrix, is a diagonal matrix representing expected errors for the retrieval algorithm. For each gas retrieval, the square root of the corresponding diagonal entry of $\hat{S}$ is multiplied by the VMR in the lowest layer of the atmospheric model for each retrieved gas (CH_4: 1.86 ppm, CO_2: 399 ppm, H_2O: 7,745 ppm). Using scene parameters for a 1 km flight altitude above sea level with 25.6° solar zenith and variable signal to noise ratio, this corresponds to an error of

between 0.14 and 0.55 ppm CH_4 beneath the aircraft. For CO_2, the error ranges between 6.6 to 26.4 ppm and for H_2O between 9.4 to 37.5 ppm.

5 Results

5.1 CH_4 emissions from natural gas sector

AVIRIS-NG identified over 250 CH_4 plumes during the Four Corners flight campaign (Frankenberg et al., 2016) using a linearized matched filter (Thompson et al., 2015b). The linearized matched filter models the background of radiance spectra as a multivariate Gaussian and provides a scalar value that represents the fraction of the gas target signature that perturbs the background. Because the target signature is defined as the change in radiance of the background caused by adding a unit mixing ratio length of CH_4, detected quantities are reported in mixing ratio lengths (ppm-m). This method is computationally efficient, accounts for the full covariance of background (atmosphere and surface) and instrument noise using in-scene data, providing high sensitivity to local enhancements.

The current speed of the IMAP-DOAS retrieval algorithm precludes it from being applied to all 250 examples presented in the previous study (Frankenberg et al., 2016). Instead, IMAP-DOAS retrievals for only a few examples will be presented here, reflecting CH_4, CO_2, and H_2O plumes from a variety of emission sources. The first example from a 20 April 2015 flight at 1.1 km AGL (Figure 3b) is made up of at least 10 plumes with maximum enhancements in excess of 5,000 ppm·m, which is equivalent to a concentration of 0.5 % in a 1 m thick layer or roughly an XCH4 (dry air column-averaged mole fraction) enhancement of around 500 ppb that is almost 25 % of a total background column. Results from the H_2O retrieval (Figure 3e) do not indicate enhancements collocated with CH_4 plumes. The true color image subset in Figure 3a reveals a few dirt roads, however, the close up of the AVIRIS-NG scene indicated by the black boxes in Figure 3a, b indicates some visible infrastructure that is difficult to interpret at the 1 m AVIRIS-NG pixel resolution (Figure 3c).

In Figure 3d, Google Earth imagery for the same area provides improved spatial resolution and reveals what appears to be drilling rigs at an active underground coal mine on 15 March 2015, suggesting the origin of these plumes are mine workings ventilation shafts. Frankenberg et al. (2016) estimated an aggregate flux of 2,236 kg hr^{-1} for these plumes. Measured and modeled radiance is shown for one image pixel within the CH_4 plume for the CH_4 retrieval fitting window (Figure 4a) and for the H_2O retrieval (Figure 5a). For both examples, the residuals are also plotted (Figure 4b, Figure 5b) in addition to the 1 σ standard deviation boundary calculated from residuals for the entire scene.

Additional examples are presented in Appendix A, including from another 20 April 2015 flight at 1.4 km AGL that results in a 1.2 m resolution (Figure 9b). Multiple CH_4 plumes are visible from this gas processing facility, one emanating from a source beyond the east edge of the AVIRIS-NG scene. This example was associated with a planned maintenance operation, which resulted in a large temporary CH_4 plume that was recorded and reported through the normal Greenhouse Gas Reporting Program (Williams, 2016). A second plume is visible at a location shown by the black box in Figure 9a), indicating white pipes associated with an interstate pipeline as the likely emission source (Figure 9c and d).

An H_2O retrieval was also performed for this scene and did not reveal enhancements collocated with the CH_4 plumes. For all subsequent examples, H_2O retrievals were performed but will be shown only in cases where H_2O plumes were observed (see Section 5.3). As shown in Figure 9a, the CH_4 plumes cross over many land cover types with variable brightness and very dark surfaces resulted in anomalously high retrievals. CH_4 results from radiances less than 0.01 μWcm^{-2} sr^{-1} nm^{-1} for any band of the CH_4 fitting window, corresponding to shadows and water, were removed from the results shown in Figure 9b.

In Figure 10b and e, CH_4 emissions from a tank were observed on 19 and 21 April 2015 at 2.8 and 3.2 km AGL (pixel resolutions of 2.6 and 3.0 m respectively). The Google Earth close up shown in Figure 10d indicates a tank as the likely emission source, which was confirmed by the ground crew using a thermal imaging camera on multiple days. Video A1 (see supplement) was acquired on 21 April 2015 at around 18:00 UTC and clearly shows a CH_4 plume originating at the top of the tank that is consistent with the AVIRIS-NG CH_4 plume observed the same day.

In Frankenberg et al. (2016), CH_4 emissions from a pipeline leak were presented (see Figure 4 and Movie S2 (Frankenberg et al., 2016)) and subsequent to publication another suspected pipeline leak (Figure S6 (Frankenberg et al., 2016)) was confirmed (Karen Spray, Department of Energy, personal communication, 2016). That leak was independently identified and repaired by the operator as a part of their normal operations prior to publication. In Figure 11b, the CH_4 plume from the 19 April 2015 flight at 3.0 km AGL (2.7 m pixel resolution) does not appear associated with visible infrastructure and subsequent investigation by the ground crews identified the plume origin on 24 April 2015 using the thermal camera (Video A2, see supplement). This location was along a marked, buried natural gas pipeline and was subsequently confirmed as a pipeline leak and ultimately shut down for repairs by the local pipeline operators. The estimated flux for this example is 28 kg hr^{-1} Frankenberg et al. (2016) which would result in an estimated annual loss of 13.2 million cubic feet, equivalent to 100,000 USD (assuming constant annual flux and average cost of 7.40 USD per thousand cubic feet).

5.2 Geological CH_4 emissions

AVIRIS has been used for quantitative retrievals of CH_4 for marine seeps (Roberts et al., 2010; Thorpe et al., 2014) and more recently a plume observed with AVIRIS-NG was verified as a geological source (see Figure S6 in Frankenberg et al. (2016)). Subsequent analysis of the Four Corners data set revealed another CH_4 plume from a confirmed geological source at Moving Mountain near Durango, Colorado (LTE, 2015). This AVIRIS-NG scene was acquired at 1.3 km AGL (1 m pixel resolution) and shows a 10 m long plume (Figure 6b).

5.3 CO_2 and H_2O emissions from power plants

While Dennison et al. (2013) demonstrated the ability of AVIRIS for high resolution mapping of CO_2 plumes, in this study we present two examples using quantitative retrievals. The first example is from the coal-fired San Juan Generating Station near Farmington, New Mexico that was flown on 20 April 2015 at 1.2 km AGL. Two CO_2 plumes are clearly visible in Figure 7b and correspond to two flue-gas stacks that appear active given visible emissions in the true color image (Figure 7a, c). A third flue-gas stack appears inactive (Figure 7a) with no visible CO_2 plume (Figure 7b). The San Juan Generating Station

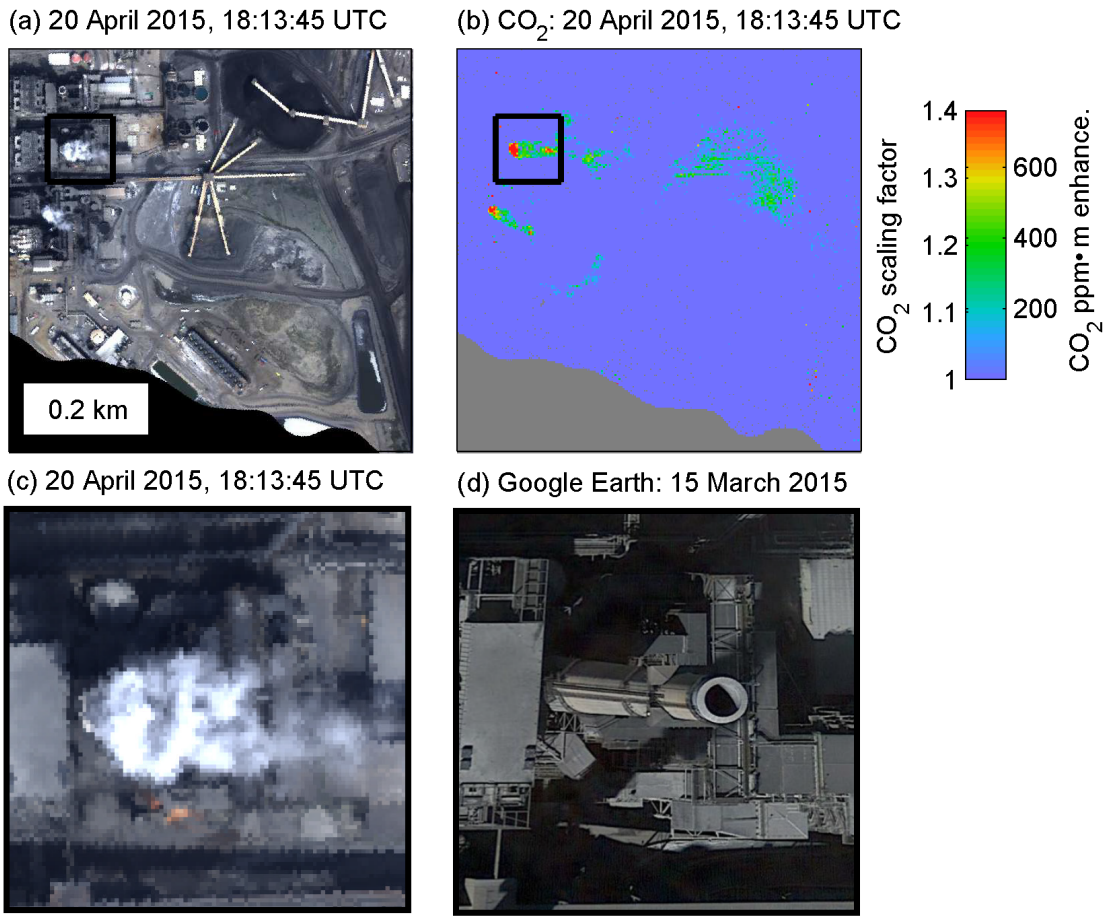

Figure 7. (a) AVIRIS-NG true color image subset. (b) CO_2 plume is visible. (c) Close up of AVIRIS-NG true color image. (d) Higher resolution Google Earth imagery provides additional spatial context. For all images, north is up.

reported 2015 emissions of 9,843 kt of CO_2, equivalent to a flux of 1,123,666 kg CO_2 hr^{-1} (EPA, 2016b). An example of a CO_2 retrieval fit and the residual is shown in (Figure 8).

The second example is from a 12 September 2014 flight that included the coal-fired Craig Station near Craig, Colorado. CO_2 plumes are visible from flue-gas stacks (Figure 12b) and extend more than 1 km downwind. This power plant reported 2014 emissions of 9,300 kt of CO_2, equivalent to a flux of 1,061,644 kg CO_2 hr^{-1} (EPA, 2016b). Within the same scene, an H_2O plume is also visible (Figure 12d) emanating from a region that contains a number of cooling towers adjacent to two large cooling ponds (Figure 13a). CH_4 retrieval results are also shown in Figure 13c indicating CH_4 plumes are not visible in the scene and emphasizing the ability of these retrievals to distinguish between CH_4 and H_2O despite spectral interference (see Figure 1). Results for dark surfaces like the cooling ponds were removed from Figure 12b by excluding radiances less than 0.10 $\mu Wcm^{-2}\,sr^{-1}\,nm^{-1}$ for any band of the CO_2 fitting window, for radiances less than 0.002 $\mu Wcm^{-2}\,sr^{-1}\,nm^{-1}$ for any

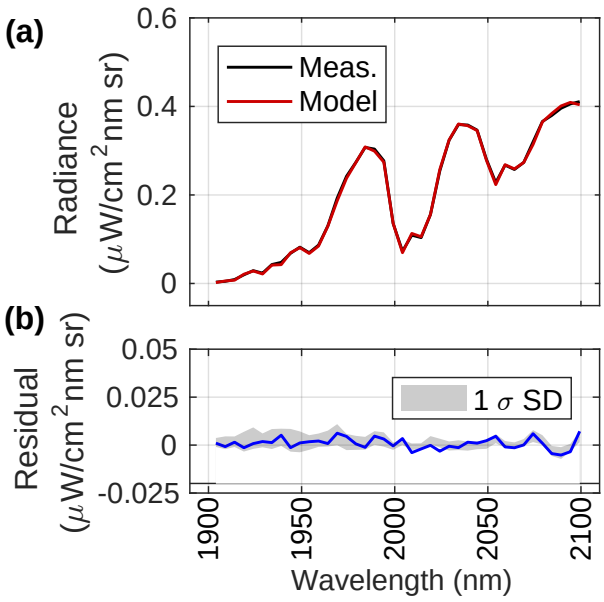

Figure 8. (a) AVIRIS-NG measured and modeled radiance for one image pixel within the CO_2 plume for the CO_2 retrieval (see Figure 7b). (b) The residual is plotted with 1 $\boldsymbol{\sigma}$ standard deviation boundary calculated from residuals for the entire scene.

band of the H_2O fitting window (Figure 12d), and for radiances less than 0.01 μWcm^{-2} sr^{-1} nm^{-1} for any band of the CH_4 fitting window (Figure 12c).

In Figure 13a, the AVIRIS-NG true color image is shown for the close up indicated by the black box in Figure 12. The flue-gas stacks are visible in the lower left as CO_2 sources and cooling towers in the upper right as possible H_2O sources. Ellipses delineate the shapes of plumes visible in the true color images for the flue-gas stacks (red) and cooling towers (blue). The arrows indicate winds to the southeast for the flue-gas stacks (consistent with CO_2 plumes in Figure 12b) and to the east for the cooling towers (consistent with H_2O plumes in Figure 12d). In 13b, the higher resolution Google Earth imagery clearly indicates the flue-gas stacks are much taller (182 m) than the cooling tower (TRI, 2016) based on assessment of shadows, which could explain variable wind directions at the flue-gas stacks and in the vicinity of the cooling towers. Given the presence of the cooling ponds immediately adjacent to the cooling towers, it is unclear if the observed H_2O plume shown in Figure 12d is caused solely by the cooling towers or reflects the combined influence of the towers and evaporation from the cooling ponds.

6 Conclusions

In this study, we use the airborne imaging spectrometer AVIRIS-NG and the Iterative Maximum a Posteriori Differential Optical Absorption Spectroscopy (IMAP-DOAS) retrieval to generate gas concentration maps for observed CH_4, CO_2, and H_2O plumes. While more than 250 CH_4 plumes were observed in the San Juan Basin near Four Corners (Frankenberg et al.,

2016), this study focused on a few results from anthropogenic and natural sources, including emissions from mine ventilation shafts, a gas processing plant, tank, pipeline leak, and natural seep. In addition, CO_2 emissions were observed from the flue-stacks of two coal-fired power plants and an H_2O plume was mapped for the cooling towers for one power plant. Observed plumes were consistent with known and suspected emission sources verified by true color AVIRIS-NG imagery and higher resolution Google Earth imagery.

AVIRIS-NG has the high spatial resolution necessary to resolve small-scale emissions and can map large regions quickly, covering the 2,500 km^2 Four Corners study in approximately two days (9.2 flight hours). This capability is aided by real time detection and geolocation of gas plumes, permitting unambiguous identification of individual emission source locations and communication to ground teams for rapid follow up. This permitted verification of a number of emission sources presented in this study using a thermal camera, including a tank and buried natural gas pipeline. The AVIRIS and AVIRIS-NG instruments have demonstrated CH_4 plume mapping capabilities at multiple flight altitudes, ranging from as low as 0.4 km to 3.8 km AGL (0.4 to 3.8 m pixels) for a controlled release experiment (Thorpe et al., 2016a) to 9 km AGL for the Coal Oil Point marine seeps (Thorpe et al., 2014). AVIRIS observed the Aliso Canyon leak on multiple flight days at 6.6 km AGL (6.6 m pixels) while the Hyperion imaging spectrometer, also 10 nm spectral resolution but 30 m pixels, mapped the plume and demonstrated the potential for a space-based application (Thompson et al., 2016).

This study demonstrates a comprehensive greenhouse gas monitoring capability that targets CH_4 and CO_2, the two dominant anthropogenic climate-forcing agents. The ability to identify individual point source locations of CH_4 and CO_2 emissions has relevance to the research community as well as the private sector. Understanding the spatial and temporal distribution as well as the magnitude of these emissions is of interest given the large uncertainties associated with anthropogenic emissions. This includes industrial point source emissions of CH_4 and CO_2, CH_4 from oil and gas operations as well as natural gas distribution and storage, CH_4 from agricultural sources, and CH_4 and CO_2 from landfills. Site operators could identify and mitigate CH_4 emissions, which reflect both a potential safety hazard and lost revenue. Water vapor results demonstrate the ability of these retrievals to distinguish between CH_4 and H_2O despite spectral interference in the short wave infrared while offering the potential to improve atmospheric correction and reflectance retrievals with application to the fields of ecology and meteorology.

Despite these promising results, an imaging spectrometer built exclusively for quantitative mapping of gas plumes would have improved sensitivity compared to AVIRIS-NG (Thorpe et al., 2014). For example, an instrument providing a 1 nm spectral resolution and sampling (2,000-2,400 nanometers) would permit mapping CH_4, CO_2, H_2O, CO, and N_2O from more diffuse sources using both airborne and orbital platforms (Thorpe et al., 2016b) . The ability to identify emission sources offers the potential to constrain regional greenhouse gas budgets and improve partitioning between anthropogenic and natural emission sources. Because the CH_4 lifetime is only about 9 years and CH_4 has a high Global Warming Potential, targeting reductions in anthropogenic CH_4 emissions offers an effective approach to decrease overall atmospheric radiative forcing.

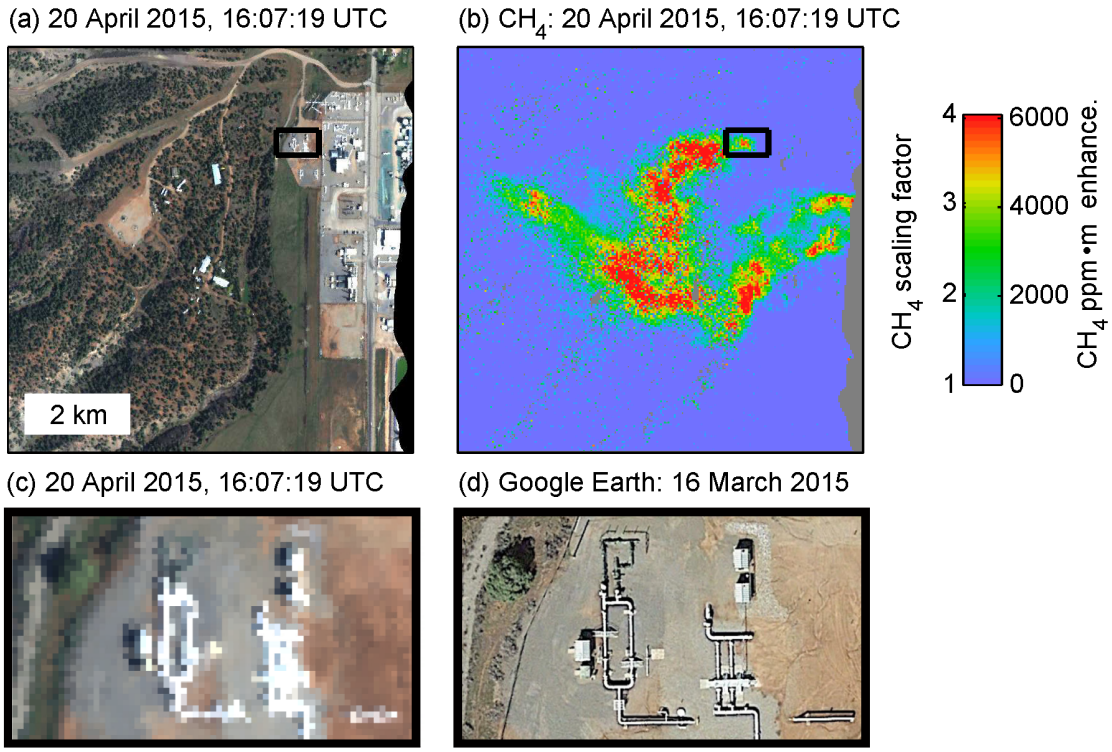

Figure 9. (a) AVIRIS-NG true color image subset. (b) Multiple CH_4 plumes are visible from this gas processing facility, one emanating from a source beyond the east edge of the AVIRIS-NG scene. A second plume is visible at a location shown by the black box. (c) Close up of AVIRIS-NG true color image indicates white pipes associated with an interstate pipeline as the likely emission source. (d) Higher resolution Google Earth imagery provides additional spatial context. For all images, north is up.

7 Data availability

The AVIRIS-NG data used in this study are available upon request at http:// avirisng.jpl.nasa.gov/ or http://aviris.jpl.nasa.gov/.

Appendix A

This appendix contains additional figures referenced in Section 5.

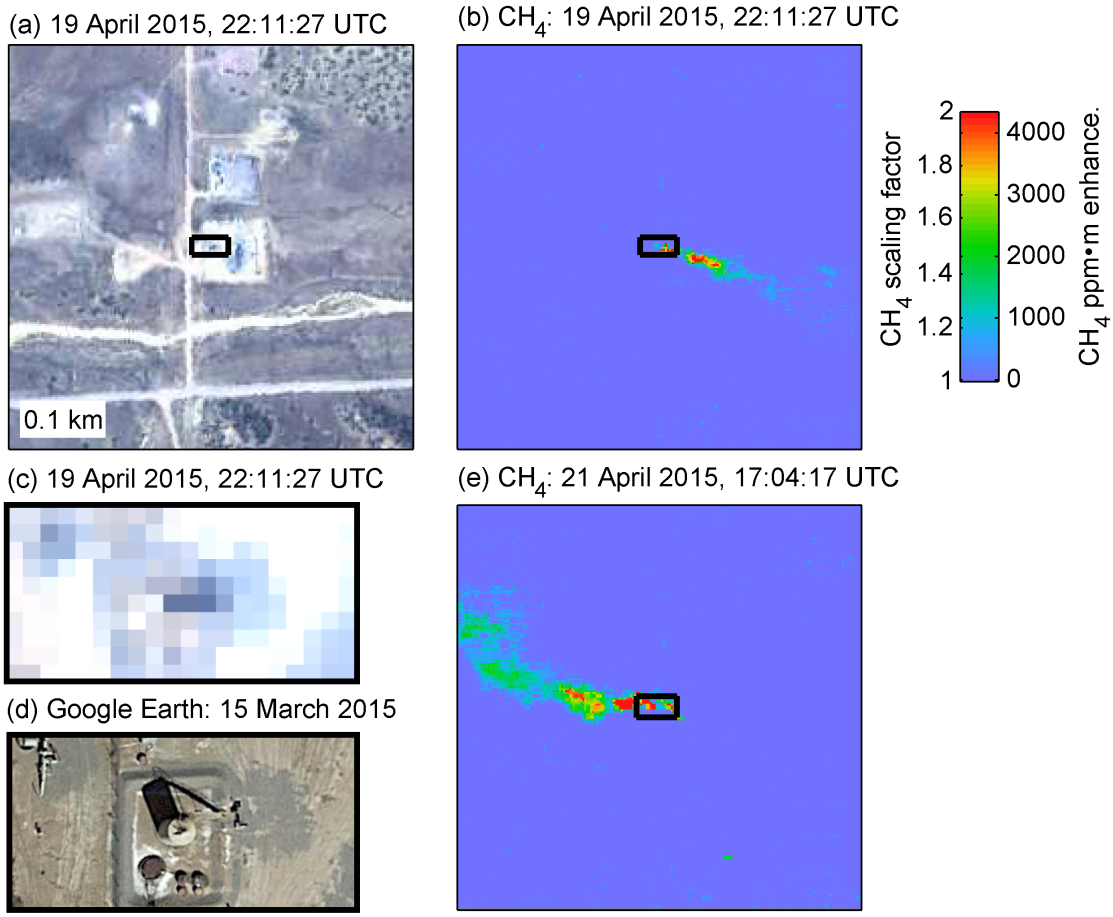

Figure 10. (a) 19 April 2015 AVIRIS-NG true color image subset. (b) Prominent CH_4 plume visible from location indicated by the black box. (c) Close up of 19 April 2015 AVIRIS-NG true color image. (d) Higher resolution Google Earth imagery indicates the emission source is a tank. (e) 21 April 2015 scene indicates a CH_4 plume from the same source with an different orientation due to changes in wind direction. For all images, north is up. A thermal camera video for this source is shown in Video A1.

A1 CH_4 emissions from gas processing facility

A2 CH_4 emissions from tank

A3 CH_4 emissions from pipeline leak

A4 CO_2 and H_2O emissions from power plant

Author contributions. C.F., A.K.T. designed research; C.F., A.D.A., A.K.T., D.R.T., B.D.B., R.O.G., E.A.K., C.S., S.C. flight campaign support; A.K.T, C.F., D.R.T., K.G., T.K., J.B. performed research, R.M.D., R.O.G, K.G., T.K., J.B., D.A.R., P.E.D. advised research, A.K.T. and C.F. analyzed data and wrote the paper.

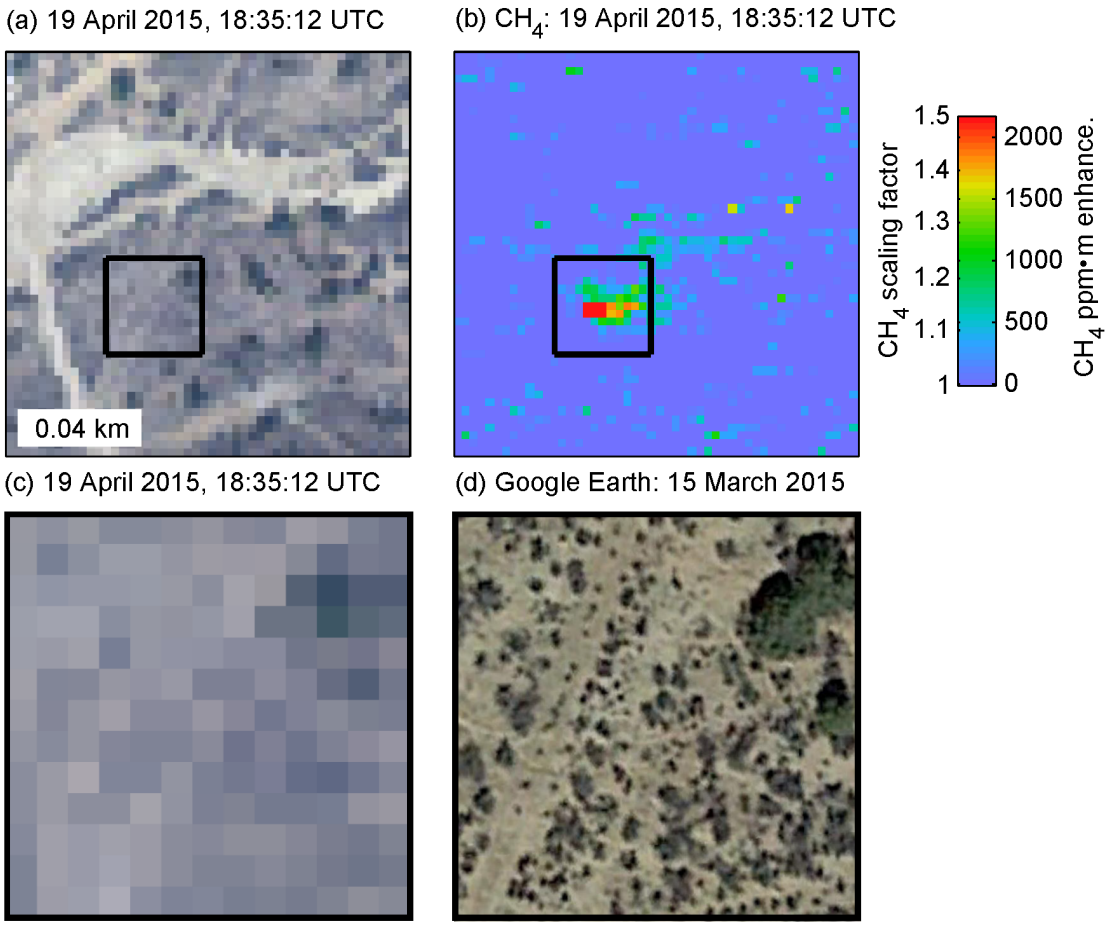

Figure 11. (a) AVIRIS-NG true color image subset. (b) A CH_4 plume is visible for a confirmed leak from a buried natural gas pipeline. (c) Close up of AVIRIS-NG true color image. (d) Higher resolution Google Earth imagery does not indicate visible infrastucture. For all images, north is up. A thermal camera video for this source is shown in Video A2.

Competing interests. The authors declare that they have no conflict of interest.

Acknowledgements. The authors thank NASA HQ and Jack Kaye for funding the flight campaign. We would like to acknowledge the contributions of the AVIRIS-NG flight and instrument teams, including Michael Eastwood, Sarah Lundeen, Ian Mccubin, Mark Helmlinger, Scott Nolte, and Betina Pavri. We would also like to thank Simon Hook and Bill Johnson for their support and for the use of the thermal camera. This work was undertaken in part at the Jet Propulsion Laboratory, California Institute of Technology under contract with NASA.
Copyright 2016. All rights reserved.

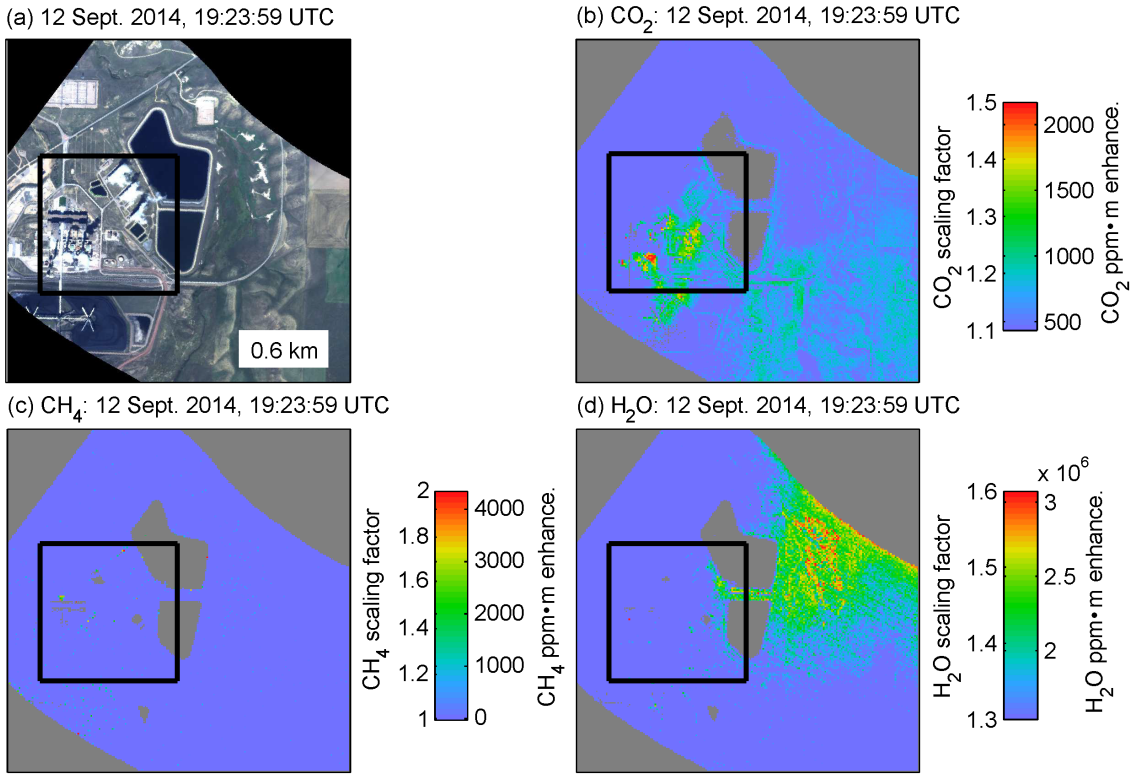

Figure 12. (a) AVIRIS-NG true color image subset. (b) CO_2 plumes are visible emanating from flue-gas stacks. (c) CH_4 retrieval results. (d) H_2O plume visible from cooling towers (see Figure 13). For all images, north is up.

References

Aubrey, A., Frankenberg, C., Green, R., Eastwood, M., Thompson, D., and Thorpe, A.: Crosscutting airborne remote sensing technologies for oil and gas and earth science applications, Offshore Technology Conference, doi:10.4043/25984-MS, 2015.

Ballantyne, A. P., Andres, R., Houghton, R., Stocker, B. D., Wanninkhof, R. amd Anderegg, W., Cooper, L. A., DeGrandpre, M., P., T. P., Miller, J. B., Alden, C., and White, J. W. C.: Audit of the global carbon budget: estimate errors and their impact on uptake uncertainty, Biogeosciences, 12, 2565–2584, doi:10.5194/bg-12-2565-2015, 2015.

Bovensmann, H., Burrows, J. P., Buchwitz, M., Frerick, J., Noel, S., Rozanov, V. V., Chance, K. V., and Goede, A. P. H.: SCIAMACHY: Mission Objectives and Measurement Modes, Journal of the Atmospheric Sciences, 56, 127–150, doi:10.1175/1520-0469(1999)056<0127:SMOAMM>2.0.CO;2, 1999.

Brandt, A. R., Heath, G. A., Kort, E. A., O'Sullivan, F., Pétron, G., Jordaan, S. M., Tans, P., Wilcox, J., Gopstein, A. M., Arent, D., Wofsy, S., Brown, N. J., Bradley, R., Stucky, G. D., Eardley, D., and Harriss, R.: Methane leaks from North American natural gas systems, Science, 343, 733–735, doi:10.1126/science.1247045, 2014.

Brandt, A. R., Heath, G. A., and Cooley, D.: Methane leaks from natural gas systems follow extreme distributions, Environmental Science & Technology, 50, 12 512–12 520, doi:10.1021/acs.est.6b04303, 2016.

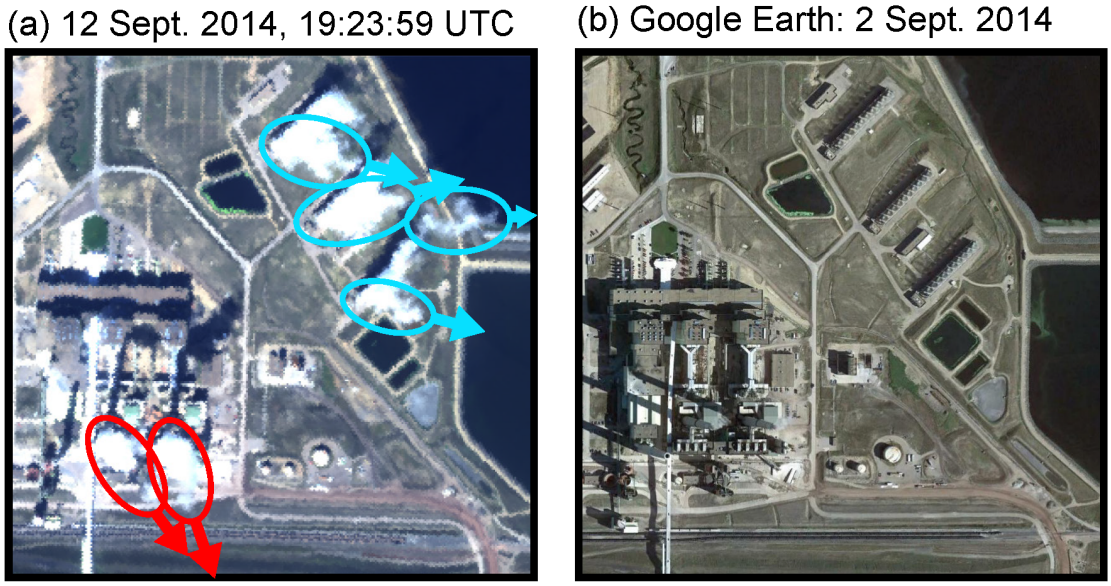

Figure 13. (a) AVIRIS-NG true color image for close up indicated by black box in Figure 12. Flue-gas stacks visible in lower left as CO_2 sources and cooling towers in upper right as H_2O sources. Ellipses delineate shapes of plumes visible in true color images for the flue-gas stacks (red) and cooling towers (blue). The arrows indicate winds to the southeast for the flue-gas stacks (consistent with CO_2 plumes in Figure 12b) and to the east for the cooling towers (consistent with H_2O plumes in Figure 12d). (b) Higher resolution Google Earth imagery clearly indicates the flue-gas stacks are much taller than the cooling towers based on assessment of shadows. For both images, north is up.

Caulton, D. R., Shepson, P. B., Santoro, R. L., Sparks, J. P., Howarth, R. W., Ingraffea, A. R., Cambaliza, M. O. L., Sweeney, C., Karion, A., Davis, K. J., Stirm, B. H., Montzka, S. A., and Miller, B. R.: Toward a better understanding and quantification of methane emissions from shale gas development, Proceedings of the National Academy of Sciences, doi:10.1073/pnas.1316546111, 2014.

Ciais, P., Crisp, D., van der Gron, H. D., Engelen, R., Janssens-Maenhout, G., Heimann, M., Rayner, P., , and Scholze, M.: Towards a European operational observing system to monitor fossil CO2 emissions, Final report from the expert group, European Comission, Tech. rep., European Comission, 2015.

Conley, S., Franco, G., Faloona, I., Blake, D. R., Peischl, J., and Ryerson, T. B.: Methane emissions from the 2015 Aliso Canyon blowout in Los Angeles, CA, Science, 351, 1317–1320, doi:10.1126/science.aaf2348, 2016.

Dennison, P. E., Thorpe, A. K., Pardyjak, E. R., Roberts, D. A., Qi, Y., Green, R. O., Bradley, E. S., and Funk, C. C.: High spatial resolution mapping of elevated atmospheric carbon dioxide using airborne imaging spectroscopy: Radiative transfer modeling and power plant plume detection, Remote Sensing of Environment, 139, 116–129, doi:10.1016/j.rse.2013.08.001, 2013.

Deschamps, A., Marion, R., Briottet, X., Foucher, P., and Lavigne, C.: Simultaneous CO2 and aerosol retrieval in a vegetation fire plume using AVIRIS hyperspectral data, doi:10.1109/WHISPERS.2011.6080896, 2011.

EIA: U.S. Energy Information Administraton, EIA annual energy outlook 2013, Tech. rep., U.S. Energy Information Administraton, 2013.

EIA: U.S. Energy Information Administraton, Top 100 U.S. oil and gas fields, Tech. rep., U.S. Energy Information Administraton, 2015.

EPA: U.S. Environmental Protection Agency, Inventory of U.S. Greenhouse Gas Emissions and Sinks: 1990–2014, Technical Report EPA 430-R-16-002 (Environmental Protection Agency), Tech. rep., U.S. Environmental Protection Agency, 2016a.

EPA: U.S. Environmental Protection Agency, 2015 Greenhouse Gas Emissions from Large Facilities, https://ghgdata.epa.gov/, Tech. rep., U.S. Environmental Protection Agency, 2016b.

Frankenberg, C., Platt, U., and Wagner, T.: Iterative maximum a posteriori (IMAP)-DOAS for retrieval of strongly absorbing trace gases: Model studies for CH4 and CO2 retrieval from near infrared spectra of SCIAMACHY onboard ENVISAT, Atmospheric Chemistry and Physics, 5, 9–22, doi:10.5194/acp-5-9-2005, 2005.

Frankenberg, C., Thorpe, A. K., Thompson, D. R., Hulley, G., Kort, E. A., Vance, N., Borchardt, J., Krings, T., Gerilowski, K., Sweeney, C., Conley, S., Bue, B. D., Aubrey, A. D., Hook, S., and Green, R. O.: Airborne methane remote measurements reveal heavy-tail flux distribution in Four Corners region, Proceedings of the National Academy of Sciences of the United States of America, 113, 9734–9739, doi:10.1073/pnas.1605617113, 2016.

Galfalk, M., Olofsson, G., Crill, P., and Bastviken, D.: Making methane visible, Nature Climate Change, 6, 426–430, doi:10.1038/nclimate2877, 2016.

Gao, B. C. and Goetz, A. F. H.: Column atmospheric water-vapor and vegetation liquid water retrievals from airborne imaging spectrometer data, Journal of Geophysical Research-Atmospheres, 95, 3549–3564, doi:10.1029/JD095iD04p03549, 1990.

Gerilowski, K., Tretner, A., Krings, T., Buchwitz, M., Bertagnolio, P. P., Belemezov, F., Erzinger, J., Burrows, J. P., and Bovensmann, H.: MAMAP - a new spectrometer system for column-averaged methane and carbon dioxide observations from aircraft: instrument description and performance analysis, Atmospheric Measurement Techniques, 4, 215–243, doi:10.5194/amt-4-215-2011, 2011.

Green, R. O., Eastwood, M. L., Sarture, C. M., Chrien, T. G., Aronsson, M., Chippendale, B. J., Faust, J. A., Pavri, B. E., Chovit, C. J., Solis, M. S., Olah, M. R., and Williams, O.: Imaging spectroscopy and the Airborne Visible Infrared Imaging Spectrometer (AVIRIS), Remote Sensing of Environment, 65, 227–248, doi:10.1016/S0034-4257(98)00064-9, 1998.

Hamlin, L., Green, R., Mouroulis, P., Eastwood, M., Wilson, D., Dudik, M., and Paine, C.: Imaging spectrometer science measurements for terrestrial ecology: AVIRIS and new developments, doi:10.1109/AERO.2011.5747395, 2011.

Hopkins, F. M., Kort, E. A., Bush, S. E., Ehleringer, J. R., Lai, C. T., Blake, D. R., and Randerson, J. T.: Spatial patterns and source attribution of urban methane in the Los Angeles Basin, Journal of Geophysical Research-Atmospheres, 121, 2490–2507, doi:10.1002/2015JD024429, 2016.

Hulley, G. C., Duren, R. M., Hopkins, F. M., Hook, S. J., Vance, N., Guillevic, P., Johnson, W. R., Eng, B. T., Mihaly, J. M., Jovanovic, V. M., Chazanoff, S. L., Staniszewski, Z. K., Kuai, L., Worden, J., Frankenberg, C., Rivera, G., Aubrey, A. D., Miller, C. E., Malakar, N. K., Tomas, J. M. S., and Holmes, K. T.: High spatial resolution imaging of methane and other trace gases with the airborne Hyperspectral Thermal Emission Spectrometer (HyTES), Atmospheric Measurement Techniques, 9, 2393–2408, doi:10.5194/amt-9-2393-2016, 2016.

Jackson, R. B., Down, A., Phillips, N. G., Ackley, R. C., Cook, C. W., Plata, D. L., and Zhao, K. G.: Natural gas pipeline leaks across Washington, DC, Environmental Science and Technology, 48, 2051–2058, doi:10.1021/es404474x, 2014.

Johnson, D. R., Covington, A. N., and Clark, N. N.: Methane Emissions from leak and loss audits of natural gas compressor stations and storage facilities, Environmental Science and Technology, 49, 8132–8138, doi:10.1021/es506163m, 2015.

Kalnay, E., Kanamitsu, M., Kistler, R., Collins, W., Deaven, D., Gandin, L., Iredell, M., Saha, S., White, G., Woollen, J., Zhu, Y., Chelliah, M., Ebisuzaki, W., Higgins, W., Janowiak, J., Mo, K. C., Ropelewski, C., Wang, J., Leetmaa, A., Reynolds, R., Jenne, R., and Joseph, D.: The NCEP/NCAR 40-year reanalysis project, Bulletin of the American Meteorological Society, 77, 437–471, doi:10.1175/1520-0477(1996)077<0437:TNYRP>2.0.CO;2, 1996.

Karion, A., Sweeney, C., Petron, G., Frost, G., Hardesty, R. M., Kofler, J., Miller, B. R., Newberger, T., Wolter, S., Banta, R., Brewer, A., Dlugokencky, E., Lang, P., Montzka, S. A., Schnell, R., Tans, P., Trainer, M., Zamora, R., and Conley, S.: Methane emissions estimate from airborne measurements over a western United States natural gas field, Geophysical Research Letters, 40, 4393–4397, doi:10.1002/grl.50811, 2013.

Kirschke, S., Bousquet, P., Ciais, P., Saunois, M., Canadell, J. G., Dlugokencky, E. J., Bergamaschi, P., Bergmann, D., Blake, D. R., Bruhwiler, L., Cameron-Smith, P., Castaldi, S., Chevallier, F., Feng, L., Fraser, A., Heimann, M., Hodson, E. L., Houweling, S., Josse, B., Fraser, P. J., Krummel, P. B., Lamarque, J. F., Langenfelds, R. L., Le Quere, C., Naik, V., O'Doherty, S., Palmer, P. I., Pison, I., Plummer, D., Poulter, B., Prinn, R. G., Rigby, M., Ringeval, B., Santini, M., Schmidt, M., Shindell, D. T., Simpson, I. J., Spahni, R., Steele, L. P., Strode, S. A., Sudo, K., Szopa, S., van der Werf, G. R., Voulgarakis, A., van Weele, M., Weiss, R. F., Williams, J. E., and Zeng, G.: Three decades of global methane sources and sinks, Nature Geoscience, 6, 813–823, doi:10.1038/ngeo1955, 2013.

Kneizys, F. X., Abreu, L. W., Anderson, G. P., Chetwynd, J. H., Shettle, E. P., Robertson, D. C., Acharya, P., Rothman, L., Selby, J. E. A., Gallery, W. O., and Clough, S. A.: The MODTRAN 2/3 report and LOWTRAN 7 model, Tech. rep., Tech. rep., Phillips Laboratory, Geophysics Directorate, 1996.

Kort, E. A., Frankenberg, C., Costigan, K. R., Lindenmaier, R., Dubey, M. K., and Wunch, D.: Four Corners: The largest US methane anomaly viewed from space, Geophysical Research Letters, p. 2014GL061503, doi:10.1002/2014GL061503, 2014.

Krautwurst, S., Gerilowski, K., Jonsson, H. H., Thompson, D. R., Kolyer, R. W., Thorpe, A. K., Horstjann, M., Eastwood, M., Leifer, I., Vigil, S., Krings, T., Borchardt, J., Buchwitz, M., Fladeland, M. M., Burrows, J. P., and Bovensmann, H.: Methane emissions from a California landfill, determined from airborne remote sensing and in-situ measurements, Atmospheric Measurement Techniques Discussions, doi:10.5194/amt-2016-391, 2016.

Krings, T., Gerilowski, K., Buchwitz, M., Reuter, M., Tretner, A., Erzinger, J., Heinze, D., Pfluger, U., Burrows, J. P., and Bovensmann, H.: MAMAP – a new spectrometer system for column-averaged methane and carbon dioxide observations from aircraft: retrieval algorithm and first inversions for point source emission rates, Atmospheric Measurement Techniques, 4, 1735–1758, doi:10.5194/amt-4-1735-2011, 2011.

Krings, T., Gerilowski, K., Buchwitz, M., Hartmann, J., Sachs, T., Erzinger, J., Burrows, J. P., and Bovensmann, H.: Quantification of methane emission rates from coal mine ventilation shafts using airborne remote sensing data, Atmospheric Measurement Techniques, 6, 151–166, doi:10.5194/amt-6-151-2013, 2013.

Kuai, L., Worden, J. R., Li, K. F., Hulley, G. C., Hopkins, F. M., Miller, C. E., Hook, S. J., Duren, R. M., and Aubrey, A. D.: Characterization of anthropogenic methane plumes with the Hyperspectral Thermal Emission Spectrometer (HyTES): A retrieval method and error analysis, Atmospheric Measurement Techniques, 9, 3165–3173, doi:10.5194/amt-9-3165-2016, 2016.

Lavoie, T. N., Shepson, P. B., Cambaliza, M. O. L., Stirm, B. H., Karion, A., Sweeney, C., Yacovitch, T. I., Herndon, S. C., Lan, X., and Lyon, D.: Aircraft-based measurements of point source methane emissions in the Barnett Shale Basin, Environmental Science & Technology, 49, 7904–7913, doi:10.1021/acs.est.5b00410, 2015.

LTE: 2015 Fruitland outcrop monitoring report ,La Plata County, Colorado, Tech. rep., LT Environmental, Inc., http://cogcc.state.co.us/documents/library/AreaReports/SanJuanBasin/3m_project/2015%20FRUITLAND%20OUTCROP%20MONITORING%20REPORT_La_Plata.pdf, 2015.

Lyon, D. R., Zavala-Araiza, D., Alvarez, R. A., Harriss, R., Palacios, V., Lan, X., Talbot, R., Lavoie, T., Shepson, P., Yacovitch, T. I., Herndon, S. C., Marchese, A. J., Zimmerle, D., Robinson, A. L., and Hamburg, S. P.: Constructing a Spatially Resolved Methane Emission Inventory for the Barnett Shale Region, Environmental Science & Technology, 49, 8147–8157, doi:10.1021/es506359c, 2015.

Marion, R., Michel, W., and Faye, C.: Measuring trace gases in plumes from hyperspectral remotely sensed data, Ieee Transactions on Geoscience and Remote Sensing, 42, 854–864, doi:10.1109/TGRS.2003.820604, 2004.

Miller, S., Wofsy, S., Michalak, A., Kort, E. A., Andrews, A., Biraud, S., Dlugockenky, E. J., Eluszkiewicz, J., Fisher, M., Janssens-Maenhout, G., Miller, B., Miller, J., Montzka, S., Nehrkorn, T., and Sweeney, C.: Anthropogenic emissions of methane in the United States, Proceedings of the National Academy of Sciences of the United States of America, 110, doi:10.1073/pnas.1314392110, 2013.

Myhre, G., Shindell, D., Bréon, F.-M., Collins, W., Fuglestvedt, J., Huang, J., Koch, D., Lamarque, J., Lee, D., Mendoza, B., Nakajima, T., Robock, A., Stephens, G., Takemura, T., and Zhang, H.: Anthropogenic and natural radiative forcing. In: Climate change 2013: The physical science basis. Contribution of Working Group I to the Fifth Assessment Report of the Intergovernmental Panel on Climate Change, Tech. rep., Intergovernmental Panel on Climate Change, 2013.

Nisbet, E. G., Dlugokencky, E. J., and Bousquet, P.: Methane on the rise—again, Science, 343, 493–495, doi:10.1126/science.1247828, 2014.

NOAA: GMD measurement locations, National Oceanic & Atmospheric Administration (NOAA), Earth System Research Laboratory, Global Monitoring Division, Tech. rep., National Oceanic & Atmospheric Administration, 2015.

NRC: National Research Council committee on methods for estimating greenhouse gas emissions; Verifying greenhouse gas emissions: Methods to support international climate agreements, The National Academies Press, Washington, D.C., 2010.

Ogunjemiyo, S., Roberts, D. A., Keightley, K., Ustin, S. L., Hinckley, T., and Lamb, B.: Evaluating the relationship between AVIRIS water vapor and poplar plantation evapotranspiration, Journal of Geophysical Research, 107, doi:10.1029/2001JD001194, 2004.

Phillips, N. G., Ackley, R., Crosson, E. R., Down, A., Hutyra, L. R., Brondfield, M., Karr, J. D., Zhao, K. G., and Jackson, R. B.: Mapping urban pipeline leaks: Methane leaks across Boston, Environmental Pollution, 173, 1–4, doi:10.1016/j.envpol.2012.11.003, 2013.

Rella, C. W., Tsai, T. R., Botkin, C. G., Crosson, E. R., and Steele, D.: Measuring emissions from oil and natural gas well pads using the mobile flux plane technique, Environmental Science & Technology, 49, 4742–4748, doi:10.1021/acs.est.5b00099, 2015.

Roberts, D. A., Bradley, E. S., Cheung, R., Leifer, I., Dennison, P. E., and Margolis, J. S.: Mapping methane emissions from a marine geological seep source using imaging spectrometry, Remote Sensing of Environment, 114, 592–606, doi:10.1016/j.rse.2009.10.015, 2010.

Rodgers, C. D.: Inverse methods for atmospheric sounding, theory and practice, World Scientific, London, 2000.

Rothman, L. S., Gordon, I. E., Barbe, A., Benner, D. C., Bernath, P. E., Birk, M., Boudon, V., Brown, L. R., Campargue, A., Champion, J. P., Chance, K., Coudert, L. H., Dana, V., Devi, V. M., Fally, S., Flaud, J. M., Gamache, R. R., Goldman, A., Jacquemart, D., Kleiner, I., Lacome, N., Lafferty, W. J., Mandin, J. Y., Massie, S. T., Mikhailenko, S. N., Miller, C. E., Moazzen-Ahmadi, N., Naumenko, O. V., Nikitin, A. V., Orphal, J., Perevalov, V. I., Perrin, A., Predoi-Cross, A., Rinsland, C. P., Rotger, M., Simeckova, M., Smith, M. A. H., Sung, K., Tashkun, S. A., Tennyson, J., Toth, R. A., Vandaele, A. C., and Vander Auwera, J.: The HITRAN 2008 molecular spectroscopic database, Journal of Quantitative Spectroscopy & Radiative Transfer, 110, 533–572, doi:10.1016/j.jqsrt.2009.02.013, 2009.

Schaefer, H., Mikaloff Fletcher, S. E., Veidt, C., Lassey, K. R., Brailsford, G. W., Bromley, T. M., Dlugokencky, E. J., Michel, S. E., Miller, J. B., Levin, I., Lowe, D. C., Martin, R. J., Vaughn, B. H., and White, J. W. C.: A 21st century shift from fossil-fuel to biogenic methane emissions indicated by 13CH4, Science, doi:10.1126/science.aad2705, 2016.

Schwietzke, S., Sherwood, O. A., Bruhwiler, L. M. P., Miller, J. B., Etiope, G., Dlugokencky, E. J., Michel, S. E., Arling, V. A., Vaughn, B. H., White, J. W. C., and Tans, P. P.: Upward revision of global fossil fuel methane emissions based on isotope database, Nature, 538, doi:10.1038/nature19797, 2016.

Smith, M. L., Kort, E. A., Karion, A., Sweeney, C., Herndon, S. C., and Yacovitch, T. I.: Airborne ethane observations in the Barnett Shale: Quantification of ethane flux and attribution of methane emissions, Environmental Science & Technology, 49, 8158–8166, doi:10.1021/acs.est.5b00219, 2015.

Thompson, D. R., Gao, B. C., Green, R. O., Dennison, P. E., Roberts, D. A., and Lundeen, S.: Atmospheric Correction for Global Mapping Spectroscopy: Advances for the HyspIRI Preparatory Campaign, Remote Sensing of Environment, 167, 64–77, doi:10.1016/j.rse.2015.02.010, 2015a.

Thompson, D. R., Leifer, I., Bovensmann, H., Eastwood, M., Fladeland, M., Frankenberg, C., Gerilowski, K., Green, R. O., Kratwurst, S., Krings, T., Luna, B., and Thorpe, A. K.: Real-time remote detection and measurement for airborne imaging spectroscopy: a case study with methane, Atmospheric Measurement Techniques, 8, 4383–4397, doi:10.5194/amt-8-4383-2015, 2015b.

Thompson, D. R., Thorpe, A. K., Frankenberg, C., Green, R. O., Duren, R., Guanter, L., Hollstein, A., Middleton, E., Ong, L., and Ungar, S.: Space-based remote imaging spectroscopy of the Aliso Canyon CH4 superemitter, Geophysical Research Letters, 43, 6571–6578, doi:10.1002/2016GL069079, 2016.

Thorpe, A., Frankenberg, C., and Roberts, D.: Retrieval techniques for airborne imaging of methane concentrations using high spatial and moderate spectral resolution: Application to AVIRIS, Atmospheric Measurement Techniques, 7, 491–506, doi:10.5194/amt-7-491-2014, 2014.

Thorpe, A. K., Frankenberg, C., Aubrey, A. D., Roberts, D. A., Nottrott, A. A., Rahn, T. A., Sauer, J. A., Dubey, M. K., Costigan, K. R., Arata, C., Steffke, A. M., Hills, S., Haselwimmer, C., Charlesworth, D., Funk, C. C., Green, R. O., Lundeen, S. R., Boardman, J. W., Eastwood, M. L., Sarture, C. M., Nolte, S. H., Mccubbin, I. B., Thompson, D. R., and McFadden, J. P.: Mapping methane concentrations from a controlled release experiment using the next generation airborne visible/infrared imaging spectrometer (AVIRIS-NG), Remote Sensing of Environment, 179, 104–115, doi:10.1016/j.rse.2016.03.032, 2016a.

Thorpe, A. K., Frankenberg, C., Green, R. O., Thompson, D. R., Aubrey, A. D., Mouroulis, P., Eastwood, M. L., and Matheou, G.: The Airborne Methane Plume Spectrometer (AMPS): Quantitative imaging of methane plumes in real time, 2016 IEEE Aerospace Conference, doi:10.1109/AERO.2016.7500756, 2016b.

Tratt, D. M., Buckland, K. N., Hall, J. L., Johnson, P. D., Keim, E. R., Leifer, I., Westberg, K., and Young, S. J.: Airborne visualization and quantification of discrete methane sources in the environment, Remote Sensing of Environment, 154, 74–88, doi:10.1016/j.rse.2014.08.011, 2014.

TRI: Tri-State Generation and Transmission Association, http://www.tsgt.coop/AboutUs/baseload-resources.cfm, Tech. rep., Tri-State Generation and Transmission Association, 2016.

Turner, A. J., Jacob, D. J., Wecht, K. J., Maasakkers, J. D., Lundgren, E., Andrews, A. E., Biraud, S. C., Boesch, H., Bowman, K. W., Deutscher, N. M., Dubey, M. K., Griffith, D. W. T., Hase, F., Kuze, A., Notholt, J., Ohyama, H., Parker, R., Payne, V. H., Sussmann, R., Sweeney, C., Velazco, V. A., Warneke, T., Wennberg, P. O., and Wunch, D.: Estimating global and North American methane emissions with high spatial resolution using GOSAT satellite data, Atmospheric Chemistry and Physics, 15, 7049–7069, doi:10.5194/acp-15-7049-2015, 2015.

Wecht, K. J., Jacob, D. J., Frankenberg, C., Jiang, Z., and Blake, D. R.: Mapping of North American methane emissions with high spatial resolution by inversion of SCIAMACHY satellite data, Journal of Geophysical Research-Atmospheres, 119, 7741–7756, doi:10.1002/2014JD021551, 2014.

Williams: NASA study shows one detection of methane in multiple surveys of Ignacio plant, Tech. rep., Williams Partners L.P., https://blog.williams.com/projects-and-operations/nasa-study-shows-no-detection-of-methane-in-multiple-surveys-of-ignacio-plant/, 2016.

Zavala-Araiza, D., Lyon, D., Alvarez, R. A., Palacios, V., Harriss, R., Lan, X., Talbot, R., and Hamburg, S. P.: Toward a functional definition of methane super-emitters: Application to natural gas production sites, Environmental Science & Technology, 49, 8167–8174, doi:10.1021/acs.est.5b00133, 2015.

Airborne DOAS retrievals of methane, carbon dioxide, and water vapor concentrations at high spatial resolution: application to AVIRIS-NG

Andrew K. Thorpe [1], Christian Frankenberg [2,1], David R. Thompson [1], Riley M. Duren [1], Andrew D. Aubrey [1], Brian D. Bue [1], Robert O. Green [1], Konstantin Gerilowski [3], Thomas Krings [3], Jakob Borchardt [3], Eric A. Kort [4], Colm Sweeney [5], Stephen Conley [6,7], Dar A. Roberts [8], and Philip E. Dennison [9]

[1]Jet Propulsion Laboratory, California Institute of Technology, Pasadena, California, United States
[2]California Institute of Technology, Pasadena, California, United States
[3]Institute of Environmental Physics (IUP), University of Bremen, Bremen, Germany
[4]University of Michigan, Ann Arbor, United States
[5]Cooperative Institute for Research in Environmental Sciences, University of Colorado, Boulder, CO, United States
[6]Global Monitoring Division, NOAA Earth System Research Laboratory, Boulder, Colorado, United States
[7]Scientific Aviation, 3335 Airport Road, Boulder, Colorado, United States
[8]University of California, Santa Barbara, Santa Barbara, California, United States
[9]University of Utah, Salt Lake City, Utah, United States

Correspondence to: Andrew K. Thorpe (Andrew.K.Thorpe@jpl.nasa.gov)

Abstract. At local scales, emissions of methane and carbon dioxide are highly uncertain. Localized sources of both trace gases can create strong local gradients in its columnar abundance, which can be discerned using absorption spectroscopy at high spatial resolution. In a previous study, more than 250 methane plumes were observed in the San Juan Basin near Four Corners during April 2015 using the next generation Airborne Visible/Infrared Imaging Spectrometer (AVIRIS-NG) and a linearized matched filter. For the first time, we apply the Iterative Maximum a Posteriori Differential Optical Absorption Spectroscopy (IMAP-DOAS) method to AVIRIS-NG data and generate gas concentration maps for methane, carbon dioxide, and water vapor plumes. This demonstrates a comprehensive greenhouse gas monitoring capability that targets methane and carbon dioxide, the two dominant anthropogenic climate-forcing agents. Water vapor results indicate the ability of these retrievals to distinguish between methane and water vapor despite spectral interference in the short wave infrared. We focus on selected cases from anthropogenic and natural sources, including emissions from mine ventilation shafts, a gas processing plant, tank, pipeline leak, and natural seep. In addition, carbon dioxide emissions were mapped from the flue-gas stacks of two coal-fired power plants and a water vapor plume was observed from the combined sources of cooling towers and cooling ponds. Observed plumes were consistent with known and suspected emission sources verified by the true color AVIRIS-NG scenes and higher resolution Google Earth imagery. Real time detection and geolocation of methane plumes by AVIRIS-NG provided unambiguous identification of individual emission source locations and communication to a ground team for rapid follow up. This permitted verification of a number of methane emission sources using a thermal camera, including a tank and buried natural gas pipeline.

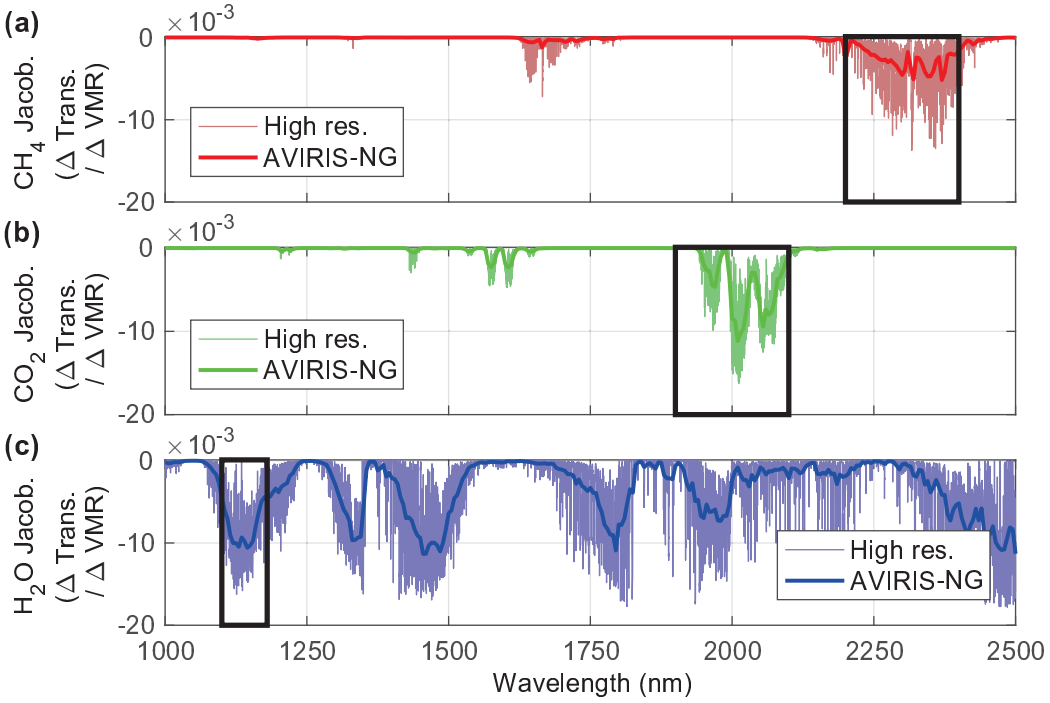

Figure 1. High resolution gas Jacobians plotted in lighter colors and for AVIRIS-NG (5 nm spectral resolution and sampling) for (a) CH_4 (red), (b) CO_2 (green), and (c) H_2O (blue). These examples were calculated for a 5 % change in CH_4 (red), (b) CO_2 (green), and (c) H_2O over the total column. AVIRIS-NG retrieval windows are indicated by the black outlines.

1 Introduction

It is important to better understand the processes controlling changes in atmospheric methane (CH_4) and carbon dioxide (CO_2), the two dominant anthropogenic climate-forcing agents. CH_4 and CO_2 contribute approximately 17 % and 64 % of the total radiative forcing attributed to anthropogenic greenhouse gases and halocarbons (Myhre et al., 2013). The atmospheric growth rates are strongly influenced by anthropogenic emissions of CH_4 and dominated by fossil fuel CO_2 emissions. Anthropogenic CH_4 sources were estimated to contribute 10.6 % of the total 2014 anthropogenic emissions of the United States, with major sources including natural gas systems (2.6 %), enteric fermentation (2.4 %), landfills (2.2 %), petroleum systems (1.0 %), coal mining (1.0 %) (EPA, 2016a). CH_4 is a precursor for tropospheric ozone and is strongly linked with co-emitted reactive trace gases that are the focus of air quality mitigation policies. U.S. anthropogenic CO_2 sources make up 81 % of the total anthropogenic emissions and are dominated by fossil fuel combustion, including electricity generation (30 %), transportation (25 %), and industrial emissions (12 %) (EPA, 2016a). U.S. emissions of both gases are projected to increase (EIA, 2013) and a number of studies have suggested that EPA bottom up emission inventories are underestimated for CH_4 (Miller et al., 2013; Wecht et al., 2014; Turner et al., 2015). U.S. fossil fuel CO_2 emissions are better constrained through existing inventories of fossil

fuel sales and combustion, however, global uncertainties are growing with the rise of a number of large, developing countries where emissions information is not readily available (NRC, 2010; Ballantyne et al., 2015; Ciais et al., 2015).

There remains uncertainty regarding the sources and sinks of atmospheric CH_4, as reflected by the ongoing scientific discussion on both the hiatus in the atmospheric growth rate in the early 21st century as well as the unexpected rise starting in 2007 (Nisbet et al., 2014). Further, regional top-down emissions estimates cannot discriminate source categories and thereby attribute fluxes to specific processes or sources. Uncertainty in anthropogenic CH_4 emissions is large at multiple scales and process attribution remains challenging because emissions originate from biological processes, venting, and leaks (Kirschke et al., 2013; Schwietzke et al., 2016; Schaefer et al., 2016).

Recent studies suggest that the majority of CH_4 emissions from oil and gas supply chains are caused by a number of super-emitters, which could explain underestimates in bottom-up inventories (Zavala-Araiza et al., 2015; Lyon et al., 2015; Brandt et al., 2014, 2016). The ability to identify emission sources offers the potential to constrain regional greenhouse gas budgets and improve partitioning between anthropogenic and natural emission sources. Although CH_4 has a short atmospheric lifetime (about 9 years), it has a very high Global Warming Potential (GWP) which is 86 times greater than CO_2 on a 20 year time scale (Myhre et al., 2013). This means that even small amounts of emissions reduction will result in large reductions in the overall atmospheric radiative forcing.

Driving surveys using in situ instruments have been used to identify CH_4 emission sources in major U.S. metropolitan areas like the Los Angeles basin (Hopkins et al., 2016), Boston (Phillips et al., 2013), and Washington, D.C. (Jackson et al., 2014) as well as to measure fluxes (Rella et al., 2015). Recently, ground-based thermal imaging systems have also been used to identify CH_4 emissions (Johnson et al., 2015; Galfalk et al., 2016). However, these methods require comprehensive sampling techniques, are time consuming, and can be limited to regions with sufficient road access. In situ airborne measurements offer the potential for increased coverage and have been used for U.S. regional CH_4 flux estimates using mass balance approaches for the Uintah Basin in northeastern Utah (Karion et al., 2013), the Marcellus formation in southwestern Pennsylvania (Caulton et al., 2014), and the Barnett Shale formation in Texas (Smith et al., 2015; Lavoie et al., 2015). These measurements reflect gas concentrations at the flight altitude and these studies are designed to estimate aggregate emissions for large regions rather than identifying individual emissions sources.

More recently, in situ airborne measurements using a chemically-instrumented Mooney aircraft have been used to estimate fluxes from known sources like the Aliso Canyon leak (Conley et al., 2016) and for a number of sources identified by imaging spectrometers in the Four Corners region (Frankenberg et al., 2016). This method samples the atmosphere directly at the flight path altitude and can measure multiple gas species. The Methane Airborne MAPper (MAMAP) spectrometer (Gerilowski et al., 2011) has also been used to measure elevated CH_4 and CO_2 column abundances to quantify emissions from a coal mine ventilation shaft (Krings et al., 2013), power plants (Krings et al., 2011), and a landfill (Krautwurst et al., 2016). MAMAP is a non-imaging spectrometer with a small field of view limited to flying transects across gas plumes rather than quickly mapping their morphology and extent on small scales. Both instruments are better suited for investigating either known emission sources or identifying larger regional emissions as opposed to individual sources.

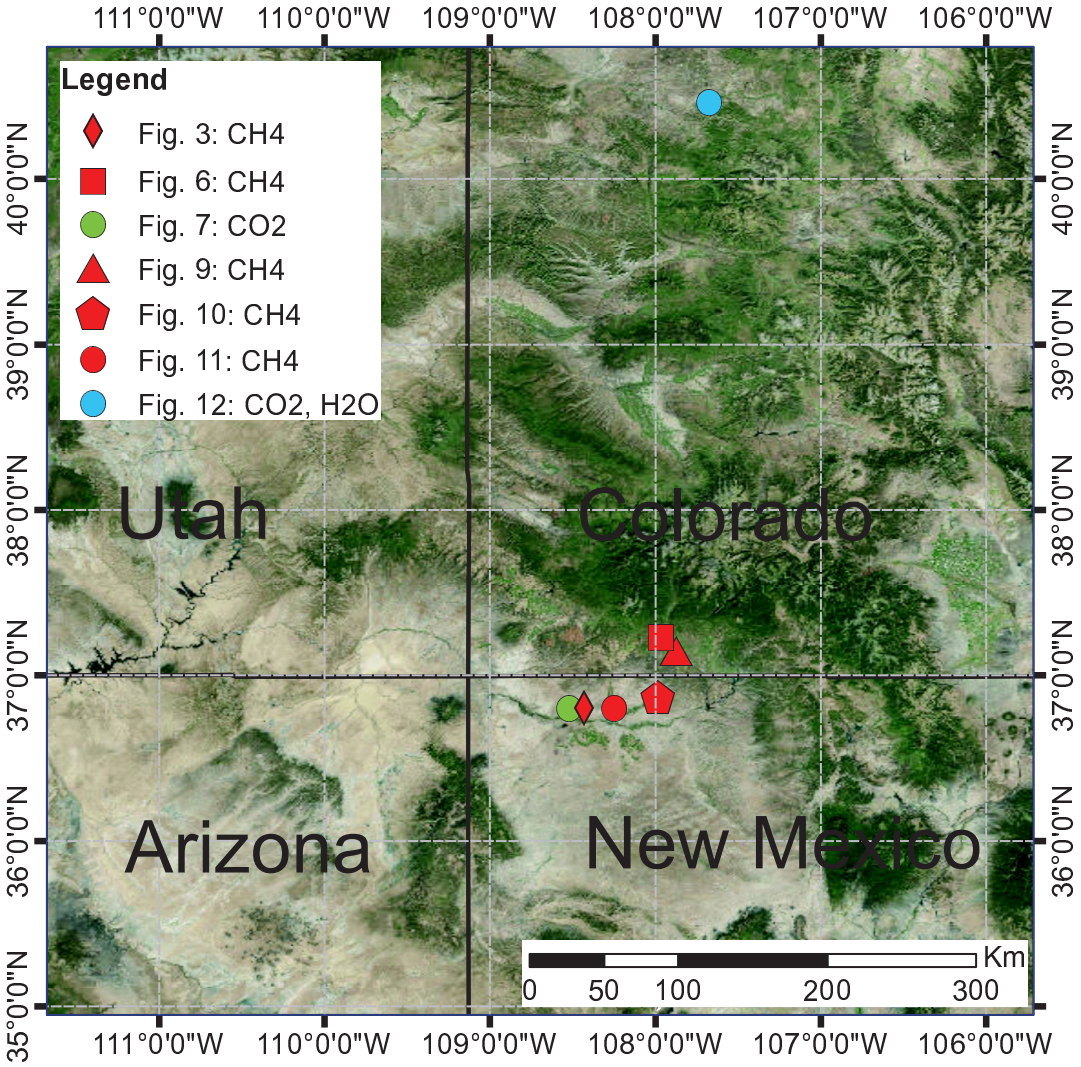

Figure 2. Locations of gas plumes presented in this study.

2 Airborne imaging spectrometers

Airborne imaging spectrometers like the Airborne Visible/Infrared Imaging Spectrometer (AVIRIS) (Green et al., 1998) and the next generation instrument AVIRIS-NG (Hamlin et al., 2011) can map large regions while providing the spatial resolution required to identify individual emissions within scenes. While not originally designed for mapping emissions, these instruments measure the 0.38 to 2.5 μm range that includes many gas absorption features (Figure 1). This has permitted quantitative retrievals of CH_4 using AVIRIS (approximately 10 nm spectral resolution and sampling) for marine seeps (Roberts et al.,

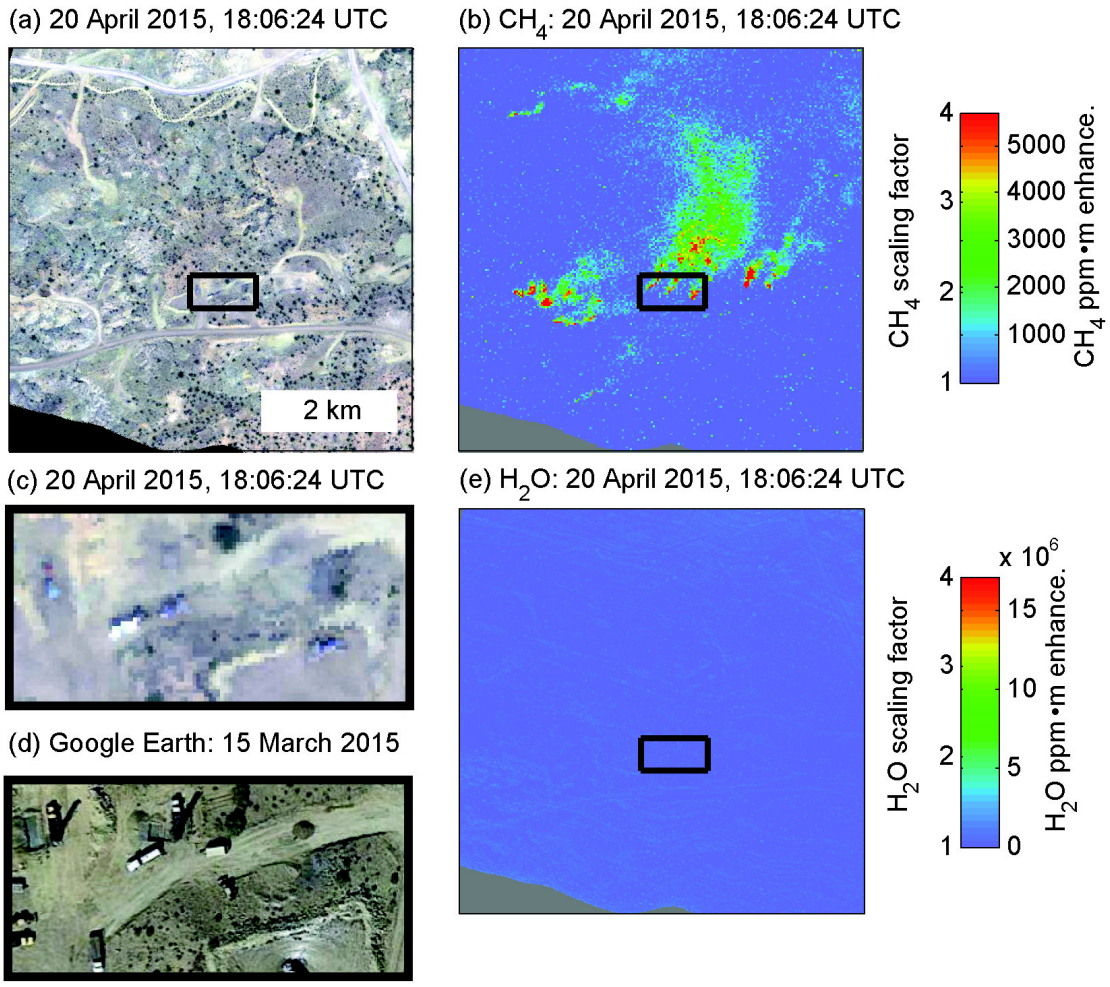

Figure 3. (a) AVIRIS-NG true color image subset. (b) A number of CH_4 plumes are clearly visible with maximum enhancements in excess of 5,000 ppm·m. (c) Close up of AVIRIS-NG true color image shown by black outline in (a). (d) Higher resolution Google Earth imagery for same area reveals drilling rigs at an active underground coal mine, suggesting the origin of these plumes are mine workings ventilation shafts. (e) H_2O retrieval does not indicate enhancements. For all images, north is up.

2010; Thorpe et al., 2014). Water vapor retrievals have been demonstrated with AVIRIS (Gao and Goetz, 1990; Thompson et al., 2015a) mainly for atmospheric correction and reflectance retrievals. However, AVIRIS water vapor retrievals have also been used to measure plant transpiration, demonstrating potential application to the fields of ecology and meteorology (Ogunjemiyo et al., 2004).

AVIRIS has been used for high resolution mapping of CO_2 plumes from industrial sources (Dennison et al., 2013) and wildfires (Marion et al., 2004; Deschamps et al., 2011). More recently, AVIRIS-NG (approximately 5 nm spectral resolution

and sampling) has surveyed large regions to identify CH_4 emissions associated with oil production (Thompson et al., 2015b), gas extraction (Frankenberg et al., 2016), hydraulic fracturing (Aubrey et al., 2015), and a landfill (Krautwurst et al., 2016). This is possible due to a 34° field of view, which results in an image swath of 1.8 km when flying at 3 km above ground level (AGL).

Airborne imaging spectrometers that operate in the thermal infrared, such as the Mako and HyTES instruments (Tratt et al., 2014; Hulley et al., 2016), have also been used for mapping CH_4 plumes. However, the altitude of maximum sensitivity varies with environmental conditions like thermal contrast (Kuai et al., 2016), which can make plumes difficult to detect and quantify, and sensitivity to near surface emissions decreases with flight altitude, which can limit ground coverage. Because AVIRIS and AVIRIS-NG measure reflected solar radiation in the short wave infrared, CH_4 retrieval sensitivity is impacted only slightly by flight altitude due to additional gas attenuation along the optical path. However, at higher flight altitude and coarser spatial resolution a gas enhancement is diluted over a larger image pixel, thereby decreasing instrument sensitivity. The ability to fly high results in more efficient flight campaigns due to improved ground coverage. For example, AVIRIS-NG consistently observed plumes for a CH_4 controlled release experiment for all altitudes flown (up to 3.8 km AGL) and AVIRIS has observed CH_4 plumes flying at 8.9 km AGL (Thorpe et al., 2014). AVIRIS has also mapped CH_4 plumes over multiple days from the Aliso Canyon leak by flying 6.6 km AGL, resulting in an image swath approximately 4.0 km wide (Thompson et al., 2016). This also offers the potential for space-based detection of emission sources, like the observed CH_4 plume from Aliso Canyon using the orbital Hyperion imaging spectrometer (Thompson et al., 2016).

In a previous study (Thorpe et al., 2014), the Iterative Maximum a Posteriori Differential Optical Absorption Spectroscopy (IMAP-DOAS) retrieval was applied to AVIRIS for quantitative mapping of CH_4 from natural and anthropogenic sources. In this study, the application of IMAP-DOAS has been expanded for use with AVIRIS-NG for multiple gas species, including CH_4, CO_2, and H_2O. We present results from AVIRIS-NG data acquired in New Mexico and Colorado, including from a flight campaign in the San Juan Basin near Four Corners. We will present results for a number of sources, including CH_4 from mine ventilation shafts, a gas processing plant, tank, pipeline leak, and natural seep, as well as CO_2 and H_2O plumes associated with power plants (Figure 2).

3 Study sites and AVIRIS-NG data

Space-based observations collected by the SCanning Imaging Absorption SpectroMeter for Atmospheric CHartographY (SCIAMACHY) instument (Bovensmann et al., 1999) showed CH_4 enhancements in the Four Corners region (Kort et al., 2014). This made for an ideal location for follow up surveys using AVIRIS-NG to identify individual emission sources. During the flight campaign, the AVIRIS-NG instrument was equipped with a real time CH_4 mapping capability using a waterfall display monitored by the instrument operator. Observed CH_4 plumes were overlaid on a true color image displaying location information as well as the maximum CH_4 enhancement (Thompson et al., 2015b). This permitted adaptive survey strategies to investigate observed plumes and the ability to send images of the plume with accurate locations to a ground crew for subsequent follow

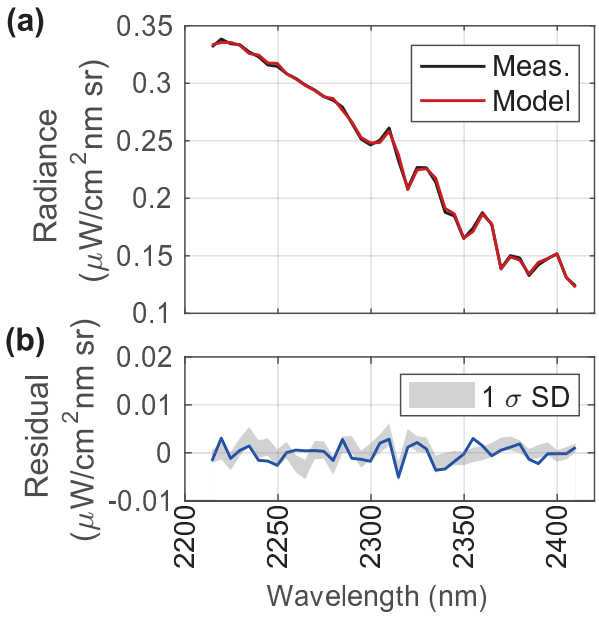

Figure 4. (a) AVIRIS-NG measured and modeled radiance for one image pixel within the CH_4 plume used for the CH_4 retrieval (see Figure 3b). (b) The residual is plotted with 1 σ standard deviation boundary calculated from residuals for the entire scene.

up. A Xenics Onca-VLWIR-MCT-384 thermal imaging camera with a Spectrogon optical filter centered at 7.746 μm was used by the ground crew to verify a number of plumes observed in real time by AVIRIS-NG.

Located in New Mexico and Colorado, the San Juan Basin produces natural gas from sandstone, coal bed CH_4, and shale formations and is the fourth largest U.S. gas field when it comes to total production (EIA, 2015). During a five day campaign in April 2015, AVIRIS-NG targeted an area corresponding to the highest CH_4 enhancements observed with SCIAMACHY (Frankenberg et al., 2016). A 2,500 km^2 area was covered in approximately two days (9.2 flight hours) flying at 3 km above ground level, resulting in scenes with an image swath of around 1.8 km and a ground resolution of 3 m. The remaining flight days were used for additional follow up flights and some repeat observations, sometimes at lower flight altitudes. During the campaign, a number of potential CH_4 emission sources were targeted, including infrastructure associated with natural gas production like wellpads, tanks, and gas processing plants, a coal mine, and natural coal bed CH_4 seeps. While the flight campaign focused on CH_4 sources, the coal-fired San Juan power generating station was also flown as a potential CO_2 emission source.

4 IMAP-DOAS retrievals

A detailed description of the IMAP-DOAS retrieval for AVIRIS can be found in Thorpe et al. (2014). Gas retrievals were performed on orthocorrected radiance data. Atmospheric profiles were generated by updating prior gas profiles from the U.S.

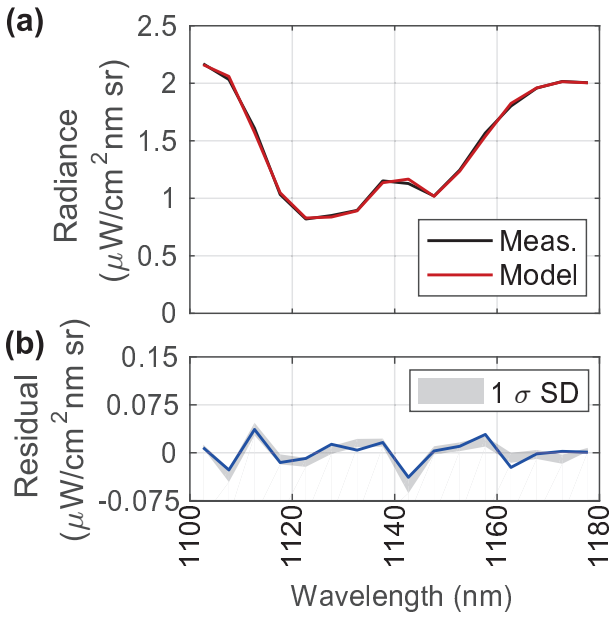

Figure 5. (a) AVIRIS-NG measured and modeled radiance for one image pixel within the CH_4 plume used for the H_2O retrieval (see Figure 3e). (b) The residual is plotted with 1 σ standard deviation boundary calculated from residuals for the entire scene.

standard atmosphere obtained from the radiative transfer models LOWTRAN/MODTRAN (Kneizys et al., 1996) using volume mixing ratios (VMR) from the NOAA Mauna Loa station, United States (NOAA, 2015). Temperature, pressure, and water vapor VMR profiles representative of the time period of the flight campaign were acquired from the National Centers for Environmental Prediction/National Center for Atmospheric Research (NCEP/NCAR) Reanalysis project (Kalnay et al., 1996). Spectral parameters for CH_4, CO_2, H_2O, and N_2O were used from the HITRAN 2008 database (Rothman et al., 2009) and a classical Voigt spectral line-shape was used to calculate vertical optical densities for fourteen atmospheric layers that spanned sea level to the top of the atmosphere.

Above the aircraft, vertical optical densities were combined and an air mass factor (AMF) was calculated to account for one way transmission. Vertical optical densities below the aircraft were also combined with an AMF reflecting two way transmission. This resulted in a two layer atmospheric model that speeds up the retrieval and incorporates the ground elevation and flight altitude for each AVIRIS-NG scene. The two layer model was used to model reflected solar radiation perturbed by the absorbing species CH_4, CO_2, H_2O, and N_2O. Three retrieval windows were used, each targeting the primary gas of interest. CH_4 retrievals were performed between 2,215 and 2,410 nm (Figure 1) and included fits for H_2O and N_2O. Gas Jacobians that reflect changes in absorption due to the absorbing species CH_4, CO_2, H_2O are shown in Figure 1. Because N_2O has weak absorption features, these Jacobians are not shown. Between 1,904 and 2,099 nm, CO_2 retrievals included H_2O and N_2O as additional unknown variables of the retrieval, while H_2O retrievals between 1,103 and 1,178 nm also included CO_2 and N_2O. Therefore, the state vector ($\boldsymbol{x}_n$) for each retrieval window has 6 entries (three gases for two atmospheric layers).

Modeled radiance at high spectral resolution was calculated for each wavelength with a forward radiative transfer model using the following equation

$$\boldsymbol{F}^{\mathrm{hr}}(\boldsymbol{x}_i) = \boldsymbol{I}_0^{\mathrm{hr}} \cdot \exp\left(-\sum_{n=1}^{6} \boldsymbol{A}_n \cdot \boldsymbol{\tau}_n^{\mathrm{ref}} \cdot \boldsymbol{x}_{n,i}\right) \cdot \sum_{i=0}^{k} a_k \lambda^k \tag{1}$$

where $\boldsymbol{F}^{\mathrm{hr}}(\boldsymbol{x}_i)$ is the forward modeled radiance at the ith iteration of the state vector, $\boldsymbol{I}_0^{\mathrm{hr}}$ is the incident intensity, a solar transmission spectrum (Geoffrey Toon, personal communication, 2013), $\boldsymbol{A}_n$ is the air mass factor (AMF) for each n number of atmospheric state vector elements, $\boldsymbol{\tau}_n^{\mathrm{ref}}$ is the reference vertical optical density for each n number of atmospheric state vector elements (including optical densities of the three absorbing species, $\boldsymbol{x}_{n,i}$ is the trace gas related state vector at the ith iteration, which scales the prior optical densities of each of the absorbing species in each n layer (six rows, three gases for two atmospheric layers), a_k are polynomial coefficients to account for low-frequency spectral variations.

The state vector contains the spectral shift (not shown here) and a low order polynomial function (a_k) to account for the broadband variability in surface albedo (see Frankenberg et al. (2005). The high resolution modeled radiance is convolved using the the instrument line shape function and sampled to the center wavelengths for each AVIRIS-NG spectral band, resulting in a lower resolution modeled radiance at the ith iteration of the state vector $\boldsymbol{F}^{\mathrm{lr}}(\boldsymbol{x}_i)$, calculated using a known $\boldsymbol{\tau}_n^{\mathrm{ref}}$ scaled by $\boldsymbol{x}_{n,i}$.

A Jacobian Matrix is calculated for each iteration i, where each column represents the derivate vector of the sensor radiance with respect to each element of the state vector ($\boldsymbol{x}_i$).

$$\mathbf{K}_i = \left.\frac{\partial \boldsymbol{F}^{\mathrm{lr}}(\boldsymbol{x})}{\partial \boldsymbol{x}}\right|_{\boldsymbol{x}_i}. \tag{2}$$

The state vector at the ith iteration can be optimized as follows (Rodgers, 2000)

$$\boldsymbol{x}_{i+1} = \boldsymbol{x}_{\mathrm{a}} + \left(\mathbf{K}_i^T \mathbf{S}_\varepsilon^{-1} \mathbf{K}_i + \mathbf{S}_{\mathrm{a}}^{-1}\right)^{-1} \mathbf{K}_i^T \mathbf{S}_\varepsilon^{-1} \cdot \left[\boldsymbol{y} - \boldsymbol{F}^{\mathrm{lr}}(\boldsymbol{x}_i) + \mathbf{K}_i(\boldsymbol{x}_i - \boldsymbol{x}_{\mathrm{a}})\right] \tag{3}$$

where $\boldsymbol{x}_{\mathrm{a}}$ is the a priori state vector (six rows), $\boldsymbol{x}_i$ is the state vector at the ith iteration (six rows), $\mathbf{S}_\varepsilon$ is the error covariance matrix, $\mathbf{S}_{\mathrm{a}}$ is the a priori covariance matrix, $\boldsymbol{y}$ is the measured AVIRIS-NG radiance, $\boldsymbol{F}^{\mathrm{lr}}(\boldsymbol{x}_i)$ is the forward model evaluated at $\boldsymbol{x}_i$, and $\mathbf{K}_i$ is the Jacobian of the forward model at $\boldsymbol{x}_i$.

The retrieval optimizes a scaling factor relative to the a priori profile. The a priori scaling factor is set to one as an initial guess for each gas in the two layers, while the a priori covariance matrix was set to constrain the fit to the atmospheric layer beneath the aircraft where high variance is expected. To do so, very small prior covariances were set for the uppermost layer (above the aircraft). Because the observed plumes are not expected to extend above the AVIRIS-NG flight altitude, this assumption is reasonable. Gas concentrations were calculated in ppm·m by multiplying the gas state vector at the last iteration (gas scaling factor) by the VMR for the lowest layer of the reference atmosphere and the distance between the aircraft and the ground. In subsequent figures, color bars will indicate the scaling factors as well as gas enhancements relative to background, which were calculated by subtracting the retrieved gas concentration from the background concentration for the lowest layer of the reference atmosphere.

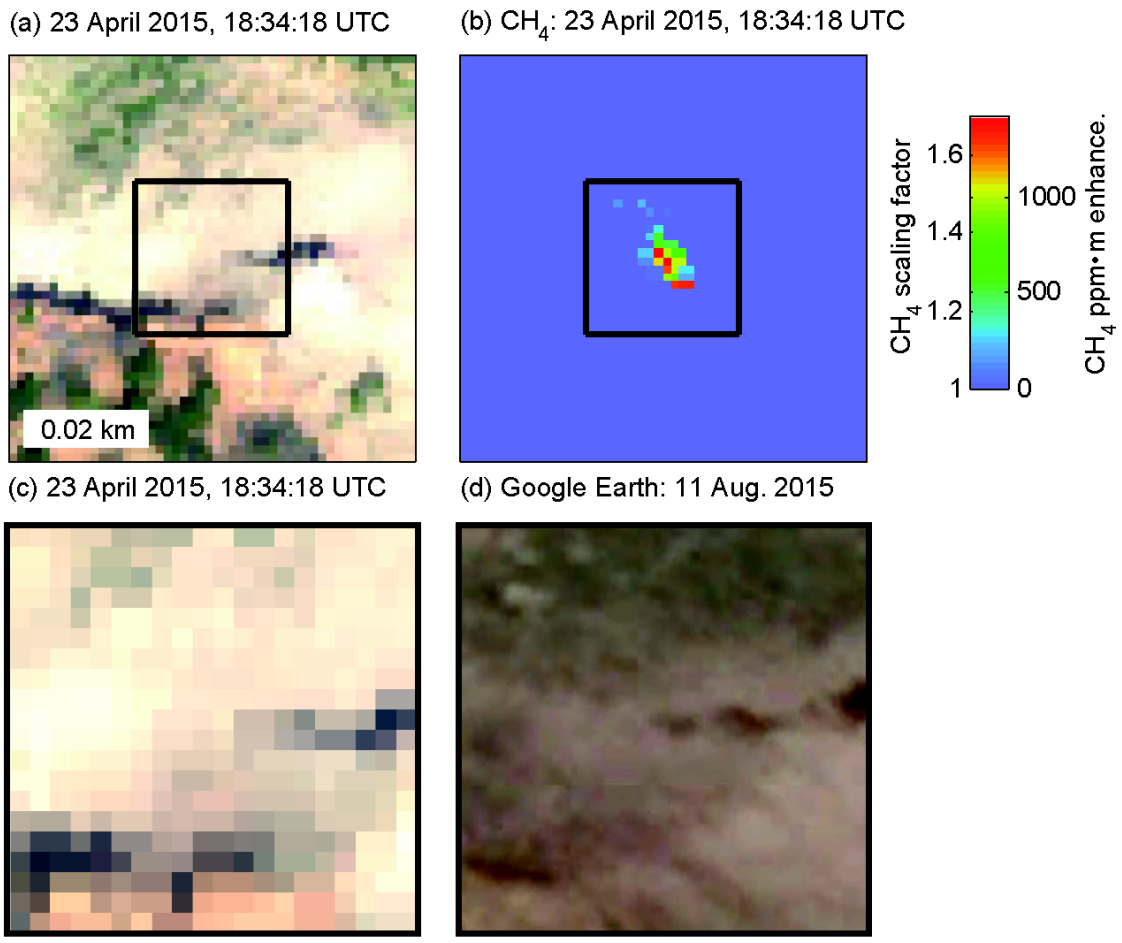

Figure 6. (a) AVIRIS-NG true color image subset. (b) A small CH_4 plume is visible from a confirmed geological source at Moving Mountain near Durango, Colorado. (c) Close up of AVIRIS-NG true color image. (d) Higher resolution Google Earth imagery provides additional spatial context. For all images, north is up.

The covariance $\hat{S}$ was calculated to estimate expected IMAP-DOAS retrieval errors as follows:

$$\hat{S} = \left(\mathbf{K}^T \mathbf{S}_\varepsilon^{-1} \mathbf{K} + \mathbf{S}_a^{-1}\right)^{-1} \tag{4}$$

where the diagonal of $\hat{S}$ corresponds to the covariance at each atmospheric layer associated with the gases used for each fitting window. $\mathbf{S}_\varepsilon$, the error covariance matrix, is a diagonal matrix representing expected errors for the retrieval algorithm. For each gas retrieval, the square root of the corresponding diagonal entry of $\hat{S}$ is multiplied by the VMR in the lowest layer of the atmospheric model for each retrieved gas (CH_4: 1.86 ppm, CO_2: 399 ppm, H_2O: 7,745 ppm). Using scene parameters for a 1 km flight altitude above sea level with 25.6° solar zenith and variable signal to noise ratio, this corresponds to an error of

between 0.14 and 0.55 ppm CH_4 beneath the aircraft. For CO_2, the error ranges between 6.6 to 26.4 ppm and for H_2O between 9.4 to 37.5 ppm.

5 Results

5.1 CH_4 emissions from natural gas sector

AVIRIS-NG identified over 250 CH_4 plumes during the Four Corners flight campaign (Frankenberg et al., 2016) using a linearized matched filter (Thompson et al., 2015b). The linearized matched filter models the background of radiance spectra as a multivariate Gaussian and provides a scalar value that represents the fraction of the gas target signature that perturbs the background. Because the target signature is defined as the change in radiance of the background caused by adding a unit mixing ratio length of CH_4, detected quantities are reported in mixing ratio lengths (ppm-m). This method is computationally efficient, accounts for the full covariance of background (atmosphere and surface) and instrument noise using in-scene data, providing high sensitivity to local enhancements.

The current speed of the IMAP-DOAS retrieval algorithm precludes it from being applied to all 250 examples presented in the previous study (Frankenberg et al., 2016). Instead, IMAP-DOAS retrievals for only a few examples will be presented here, reflecting CH_4, CO_2, and H_2O plumes from a variety of emission sources. The first example from a 20 April 2015 flight at 1.1 km AGL (Figure 3b) is made up of at least 10 plumes with maximum enhancements in excess of 5,000 ppm·m, which is equivalent to a concentration of 0.5 % in a 1 m thick layer or roughly an XCH4 (dry air column-averaged mole fraction) enhancement of around 500 ppb that is almost 25 % of a total background column. Results from the H_2O retrieval (Figure 3e) do not indicate enhancements collocated with CH_4 plumes. The true color image subset in Figure 3a reveals a few dirt roads, however, the close up of the AVIRIS-NG scene indicated by the black boxes in Figure 3a, b indicates some visible infrastructure that is difficult to interpret at the 1 m AVIRIS-NG pixel resolution (Figure 3c).

In Figure 3d, Google Earth imagery for the same area provides improved spatial resolution and reveals what appears to be drilling rigs at an active underground coal mine on 15 March 2015, suggesting the origin of these plumes are mine workings ventilation shafts. Frankenberg et al. (2016) estimated an aggregate flux of 2,236 kg hr^{-1} for these plumes. Measured and modeled radiance is shown for one image pixel within the CH_4 plume for the CH_4 retrieval fitting window (Figure 4a) and for the H_2O retrieval (Figure 5a). For both examples, the residuals are also plotted (Figure 4b, Figure 5b) in addition to the 1 σ standard deviation boundary calculated from residuals for the entire scene.

Additional examples are presented in Appendix A, including from another 20 April 2015 flight at 1.4 km AGL that results in a 1.2 m resolution (Figure 9b). Multiple CH_4 plumes are visible from this gas processing facility, one emanating from a source beyond the east edge of the AVIRIS-NG scene. This example was associated with a planned maintenance operation, which resulted in a large temporary CH_4 plume that was recorded and reported through the normal Greenhouse Gas Reporting Program (Williams, 2016). A second plume is visible at a location shown by the black box in Figure 9a), indicating white pipes associated with an interstate pipeline as the likely emission source (Figure 9c and d).

An H_2O retrieval was also performed for this scene and did not reveal enhancements collocated with the CH_4 plumes. For all subsequent examples, H_2O retrievals were performed but will be shown only in cases where H_2O plumes were observed (see Section 5.3). As shown in Figure 9a, the CH_4 plumes cross over many land cover types with variable brightness and very dark surfaces resulted in anomalously high retrievals. CH_4 results from radiances less than 0.01 μWcm^{-2} sr^{-1} nm^{-1} for any band of the CH_4 fitting window, corresponding to shadows and water, were removed from the results shown in Figure 9b.

In Figure 10b and e, CH_4 emissions from a tank were observed on 19 and 21 April 2015 at 2.8 and 3.2 km AGL (pixel resolutions of 2.6 and 3.0 m respectively). The Google Earth close up shown in Figure 10d indicates a tank as the likely emission source, which was confirmed by the ground crew using a thermal imaging camera on multiple days. Video A1 (see supplement) was acquired on 21 April 2015 at around 18:00 UTC and clearly shows a CH_4 plume originating at the top of the tank that is consistent with the AVIRIS-NG CH_4 plume observed the same day.

In Frankenberg et al. (2016), CH_4 emissions from a pipeline leak were presented (see Figure 4 and Movie S2 (Frankenberg et al., 2016)) and subsequent to publication another suspected pipeline leak (Figure S6 (Frankenberg et al., 2016)) was confirmed (Karen Spray, Department of Energy, personal communication, 2016). That leak was independently identified and repaired by the operator as a part of their normal operations prior to publication. In Figure 11b, the CH_4 plume from the 19 April 2015 flight at 3.0 km AGL (2.7 m pixel resolution) does not appear associated with visible infrastructure and subsequent investigation by the ground crews identified the plume origin on 24 April 2015 using the thermal camera (Video A2, see supplement). This location was along a marked, buried natural gas pipeline and was subsequently confirmed as a pipeline leak and ultimately shut down for repairs by the local pipeline operators. The estimated flux for this example is 28 kg hr^{-1} Frankenberg et al. (2016) which would result in an estimated annual loss of 13.2 million cubic feet, equivalent to 100,000 USD (assuming constant annual flux and average cost of 7.40 USD per thousand cubic feet).

5.2 Geological CH_4 emissions

AVIRIS has been used for quantitative retrievals of CH_4 for marine seeps (Roberts et al., 2010; Thorpe et al., 2014) and more recently a plume observed with AVIRIS-NG was verified as a geological source (see Figure S6 in Frankenberg et al. (2016)). Subsequent analysis of the Four Corners data set revealed another CH_4 plume from a confirmed geological source at Moving Mountain near Durango, Colorado (LTE, 2015). This AVIRIS-NG scene was acquired at 1.3 km AGL (1 m pixel resolution) and shows a 10 m long plume (Figure 6b).

5.3 CO_2 and H_2O emissions from power plants

While Dennison et al. (2013) demonstrated the ability of AVIRIS for high resolution mapping of CO_2 plumes, in this study we present two examples using quantitative retrievals. The first example is from the coal-fired San Juan Generating Station near Farmington, New Mexico that was flown on 20 April 2015 at 1.2 km AGL. Two CO_2 plumes are clearly visible in Figure 7b and correspond to two flue-gas stacks that appear active given visible emissions in the true color image (Figure 7a, c). A third flue-gas stack appears inactive (Figure 7a) with no visible CO_2 plume (Figure 7b). The San Juan Generating Station

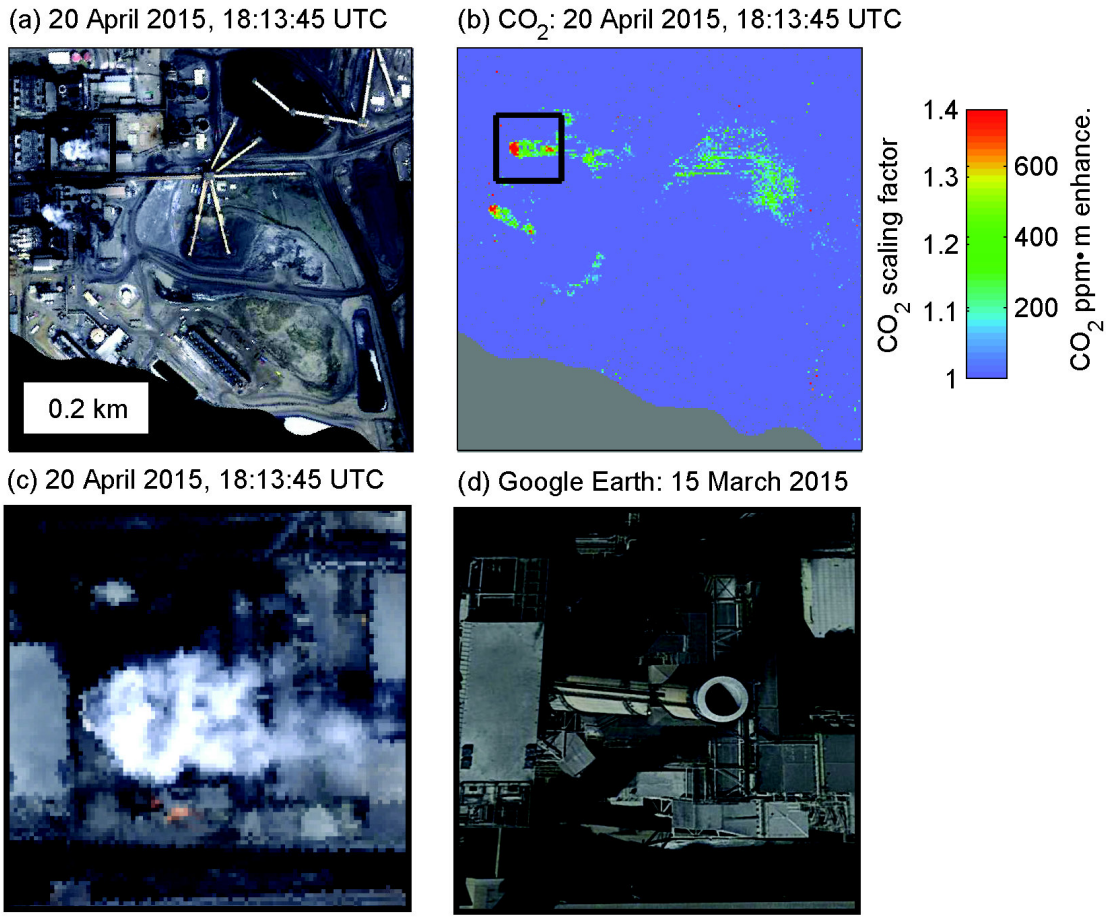

Figure 7. (a) AVIRIS-NG true color image subset. (b) CO_2 plume is visible. (c) Close up of AVIRIS-NG true color image. (d) Higher resolution Google Earth imagery provides additional spatial context. For all images, north is up.

reported 2015 emissions of 9,843 kt of CO_2, equivalent to a flux of 1,123,666 kg CO_2 hr^{-1} (EPA, 2016b). An example of a CO_2 retrieval fit and the residual is shown in (Figure 8).

The second example is from a 12 September 2014 flight that included the coal-fired Craig Station near Craig, Colorado. CO_2 plumes are visible from flue-gas stacks (Figure 12b) and extend more than 1 km downwind. This power plant reported 2014 emissions of 9,300 kt of CO_2, equivalent to a flux of 1,061,644 kg CO_2 hr^{-1} (EPA, 2016b). Within the same scene, an H_2O plume is also visible (Figure 12d) emanating from a region that contains a number of cooling towers adjacent to two large cooling ponds (Figure 13a). CH_4 retrieval results are also shown in Figure 13c indicating CH_4 plumes are not visible in the scene and emphasizing the ability of these retrievals to distinguish between CH_4 and H_2O despite spectral interference (see Figure 1). Results for dark surfaces like the cooling ponds were removed from Figure 12b by excluding radiances less than 0.10 $\mu Wcm^{-2}\,sr^{-1}\,nm^{-1}$ for any band of the CO_2 fitting window, for radiances less than 0.002 $\mu Wcm^{-2}\,sr^{-1}\,nm^{-1}$ for any

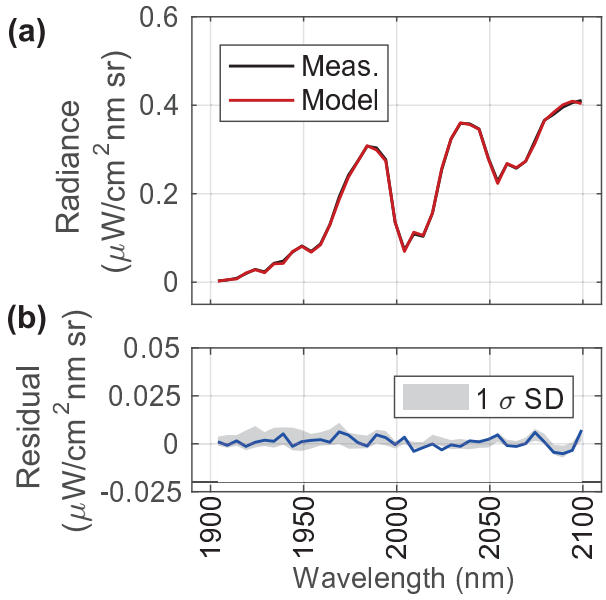

Figure 8. (a) AVIRIS-NG measured and modeled radiance for one image pixel within the CO_2 plume for the CO_2 retrieval (see Figure 7b). (b) The residual is plotted with 1 σ standard deviation boundary calculated from residuals for the entire scene.

band of the H_2O fitting window (Figure 12d), and for radiances less than 0.01 μWcm^{-2} sr^{-1} nm^{-1} for any band of the CH_4 fitting window (Figure 12c).

In Figure 13a, the AVIRIS-NG true color image is shown for the close up indicated by the black box in Figure 12. The flue-gas stacks are visible in the lower left as CO_2 sources and cooling towers in the upper right as possible H_2O sources. Ellipses delineate the shapes of plumes visible in the true color images for the flue-gas stacks (red) and cooling towers (blue). The arrows indicate winds to the southeast for the flue-gas stacks (consistent with CO_2 plumes in Figure 12b) and to the east for the cooling towers (consistent with H_2O plumes in Figure 12d). In 13b, the higher resolution Google Earth imagery clearly indicates the flue-gas stacks are much taller (182 m) than the cooling tower (TRI, 2016) based on assessment of shadows, which could explain variable wind directions at the flue-gas stacks and in the vicinity of the cooling towers. Given the presence of the cooling ponds immediately adjacent to the cooling towers, it is unclear if the observed H_2O plume shown in Figure 12d is caused solely by the cooling towers or reflects the combined influence of the towers and evaporation from the cooling ponds.

6 Conclusions

In this study, we use the airborne imaging spectrometer AVIRIS-NG and the Iterative Maximum a Posteriori Differential Optical Absorption Spectroscopy (IMAP-DOAS) retrieval to generate gas concentration maps for observed CH_4, CO_2, and H_2O plumes. While more than 250 CH_4 plumes were observed in the San Juan Basin near Four Corners (Frankenberg et al.,

2016), this study focused on a few results from anthropogenic and natural sources, including emissions from mine ventilation shafts, a gas processing plant, tank, pipeline leak, and natural seep. In addition, CO_2 emissions were observed from the flue-stacks of two coal-fired power plants and an H_2O plume was mapped for the cooling towers for one power plant. Observed plumes were consistent with known and suspected emission sources verified by true color AVIRIS-NG imagery and higher resolution Google Earth imagery.

AVIRIS-NG has the high spatial resolution necessary to resolve small-scale emissions and can map large regions quickly, covering the 2,500 km^2 Four Corners study in approximately two days (9.2 flight hours). This capability is aided by real time detection and geolocation of gas plumes, permitting unambiguous identification of individual emission source locations and communication to ground teams for rapid follow up. This permitted verification of a number of emission sources presented in this study using a thermal camera, including a tank and buried natural gas pipeline. The AVIRIS and AVIRIS-NG instruments have demonstrated CH_4 plume mapping capabilities at multiple flight altitudes, ranging from as low as 0.4 km to 3.8 km AGL (0.4 to 3.8 m pixels) for a controlled release experiment (Thorpe et al., 2016a) to 9 km AGL for the Coal Oil Point marine seeps (Thorpe et al., 2014). AVIRIS observed the Aliso Canyon leak on multiple flight days at 6.6 km AGL (6.6 m pixels) while the Hyperion imaging spectrometer, also 10 nm spectral resolution but 30 m pixels, mapped the plume and demonstrated the potential for a space-based application (Thompson et al., 2016).

This study demonstrates a comprehensive greenhouse gas monitoring capability that targets CH_4 and CO_2, the two dominant anthropogenic climate-forcing agents. The ability to identify individual point source locations of CH_4 and CO_2 emissions has relevance to the research community as well as the private sector. Understanding the spatial and temporal distribution as well as the magnitude of these emissions is of interest given the large uncertainties associated with anthropogenic emissions. This includes industrial point source emissions of CH_4 and CO_2, CH_4 from oil and gas operations as well as natural gas distribution and storage, CH_4 from agricultural sources, and CH_4 and CO_2 from landfills. Site operators could identify and mitigate CH_4 emissions, which reflect both a potential safety hazard and lost revenue. Water vapor results demonstrate the ability of these retrievals to distinguish between CH_4 and H_2O despite spectral interference in the short wave infrared while offering the potential to improve atmospheric correction and reflectance retrievals with application to the fields of ecology and meteorology.

Despite these promising results, an imaging spectrometer built exclusively for quantitative mapping of gas plumes would have improved sensitivity compared to AVIRIS-NG (Thorpe et al., 2014). For example, an instrument providing a 1 nm spectral resolution and sampling (2,000-2,400 nanometers) would permit mapping CH_4, CO_2, H_2O, CO, and N_2O from more diffuse sources using both airborne and orbital platforms (Thorpe et al., 2016b) . The ability to identify emission sources offers the potential to constrain regional greenhouse gas budgets and improve partitioning between anthropogenic and natural emission sources. Because the CH_4 lifetime is only about 9 years and CH_4 has a high Global Warming Potential, targeting reductions in anthropogenic CH_4 emissions offers an effective approach to decrease overall atmospheric radiative forcing.

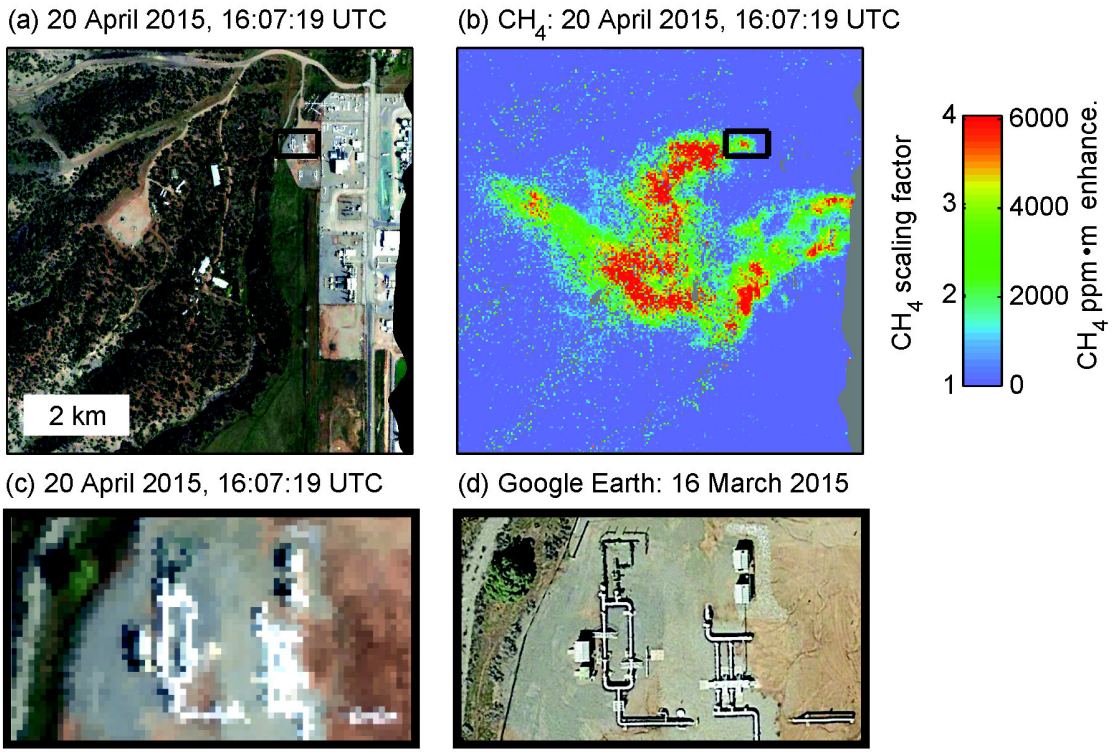

Figure 9. (a) AVIRIS-NG true color image subset. (b) Multiple CH_4 plumes are visible from this gas processing facility, one emanating from a source beyond the east edge of the AVIRIS-NG scene. A second plume is visible at a location shown by the black box. (c) Close up of AVIRIS-NG true color image indicates white pipes associated with an interstate pipeline as the likely emission source. (d) Higher resolution Google Earth imagery provides additional spatial context. For all images, north is up.

7 Data availability

The AVIRIS-NG data used in this study are available upon request at http:// avirisng.jpl.nasa.gov/ or http://aviris.jpl.nasa.gov/.

Appendix A

This appendix contains additional figures referenced in Section 5.

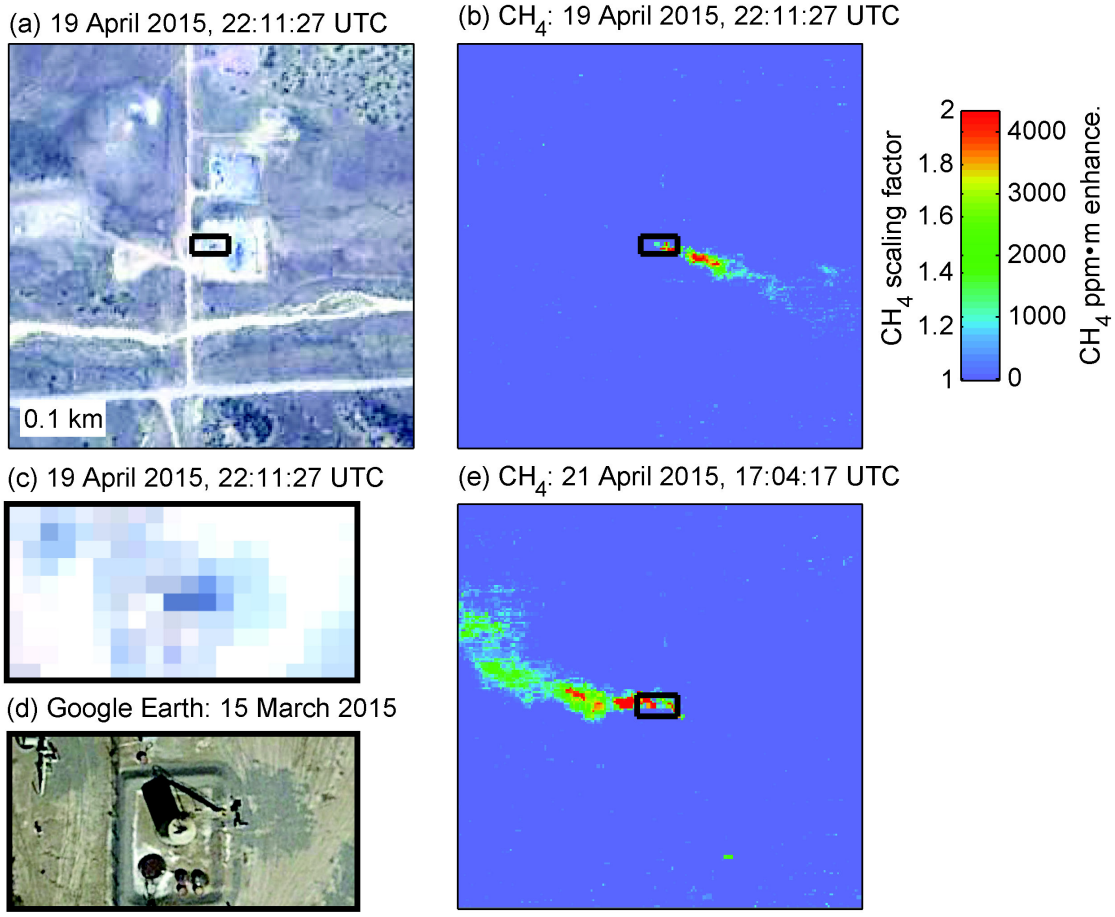

Figure 10. (a) 19 April 2015 AVIRIS-NG true color image subset. (b) Prominent CH_4 plume visible from location indicated by the black box. (c) Close up of 19 April 2015 AVIRIS-NG true color image. (d) Higher resolution Google Earth imagery indicates the emission source is a tank. (e) 21 April 2015 scene indicates a CH_4 plume from the same source with an different orientation due to changes in wind direction. For all images, north is up. A thermal camera video for this source is shown in Video A1.

A1 CH_4 emissions from gas processing facility

A2 CH_4 emissions from tank

A3 CH_4 emissions from pipeline leak

A4 CO_2 and H_2O emissions from power plant

Author contributions. C.F., A.K.T. designed research; C.F., A.D.A., A.K.T., D.R.T., B.D.B., R.O.G., E.A.K., C.S., S.C. flight campaign support; A.K.T, C.F., D.R.T., K.G., T.K., J.B. performed research, R.M.D., R.O.G, K.G., T.K., J.B., D.A.R., P.E.D. advised research, A.K.T. and C.F. analyzed data and wrote the paper.

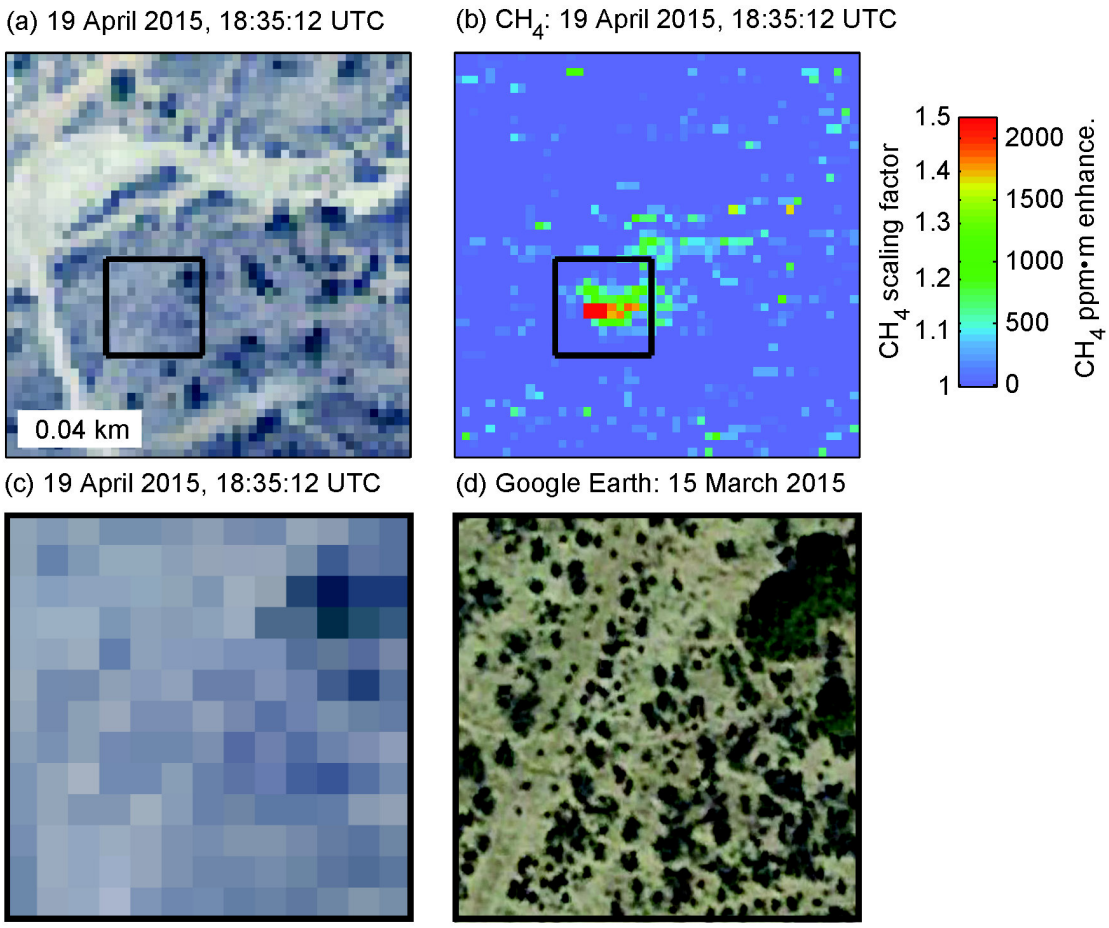

Figure 11. (a) AVIRIS-NG true color image subset. (b) A CH_4 plume is visible for a confirmed leak from a buried natural gas pipeline. (c) Close up of AVIRIS-NG true color image. (d) Higher resolution Google Earth imagery does not indicate visible infrastucture. For all images, north is up. A thermal camera video for this source is shown in Video A2.

Competing interests. The authors declare that they have no conflict of interest.

Acknowledgements. The authors thank NASA HQ and Jack Kaye for funding the flight campaign. We would like to acknowledge the contributions of the AVIRIS-NG flight and instrument teams, including Michael Eastwood, Sarah Lundeen, Ian Mccubin, Mark Helmlinger, Scott Nolte, and Betina Pavri. We would also like to thank Simon Hook and Bill Johnson for their support and for the use of the thermal camera. This work was undertaken in part at the Jet Propulsion Laboratory, California Institute of Technology under contract with NASA. Copyright 2016. All rights reserved.

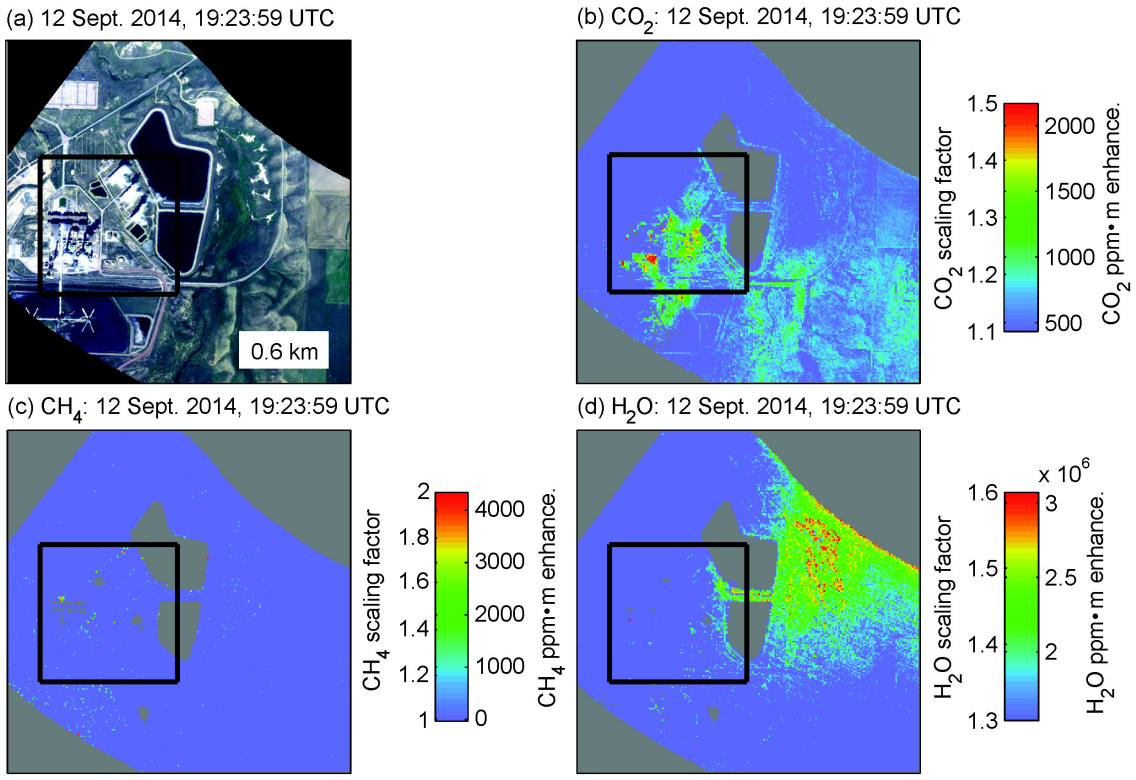

Figure 12. (a) AVIRIS-NG true color image subset. (b) CO_2 plumes are visible emanating from flue-gas stacks. (c) CH_4 retrieval results. (d) H_2O plume visible from cooling towers (see Figure 13). For all images, north is up.

References

Aubrey, A., Frankenberg, C., Green, R., Eastwood, M., Thompson, D., and Thorpe, A.: Crosscutting airborne remote sensing technologies for oil and gas and earth science applications, Offshore Technology Conference, doi:10.4043/25984-MS, 2015.

Ballantyne, A. P., Andres, R., Houghton, R., Stocker, B. D., Wanninkhof, R. amd Anderegg, W., Cooper, L. A., DeGrandpre, M., P., T. P., Miller, J. B., Alden, C., and White, J. W. C.: Audit of the global carbon budget: estimate errors and their impact on uptake uncertainty, Biogeosciences, 12, 2565–2584, doi:10.5194/bg-12-2565-2015, 2015.

Bovensmann, H., Burrows, J. P., Buchwitz, M., Frerick, J., Noel, S., Rozanov, V. V., Chance, K. V., and Goede, A. P. H.: SCIAMACHY: Mission Objectives and Measurement Modes, Journal of the Atmospheric Sciences, 56, 127–150, doi:10.1175/1520-0469(1999)056<0127:SMOAMM>2.0.CO;2, 1999.

Brandt, A. R., Heath, G. A., Kort, E. A., O'Sullivan, F., Pétron, G., Jordaan, S. M., Tans, P., Wilcox, J., Gopstein, A. M., Arent, D., Wofsy, S., Brown, N. J., Bradley, R., Stucky, G. D., Eardley, D., and Harriss, R.: Methane leaks from North American natural gas systems, Science, 343, 733–735, doi:10.1126/science.1247045, 2014.

Brandt, A. R., Heath, G. A., and Cooley, D.: Methane leaks from natural gas systems follow extreme distributions, Environmental Science & Technology, 50, 12 512–12 520, doi:10.1021/acs.est.6b04303, 2016.

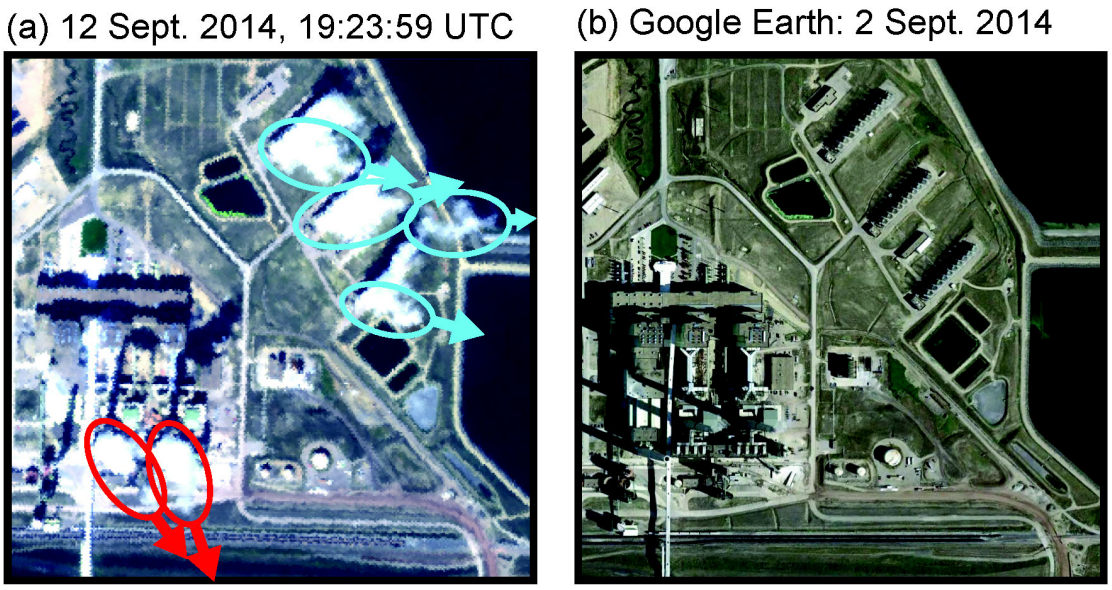

Figure 13. (a) AVIRIS-NG true color image for close up indicated by black box in Figure 12. Flue-gas stacks visible in lower left as CO_2 sources and cooling towers in upper right as H_2O sources. Ellipses delineate shapes of plumes visible in true color images for the flue-gas stacks (red) and cooling towers (blue). The arrows indicate winds to the southeast for the flue-gas stacks (consistent with CO_2 plumes in Figure 12b) and to the east for the cooling towers (consistent with H_2O plumes in Figure 12d). (b) Higher resolution Google Earth imagery clearly indicates the flue-gas stacks are much taller than the cooling towers based on assessment of shadows. For both images, north is up.

Caulton, D. R., Shepson, P. B., Santoro, R. L., Sparks, J. P., Howarth, R. W., Ingraffea, A. R., Cambaliza, M. O. L., Sweeney, C., Karion, A., Davis, K. J., Stirm, B. H., Montzka, S. A., and Miller, B. R.: Toward a better understanding and quantification of methane emissions from shale gas development, Proceedings of the National Academy of Sciences, doi:10.1073/pnas.1316546111, 2014.

Ciais, P., Crisp, D., van der Gron, H. D., Engelen, R., Janssens-Maenhout, G., Heimann, M., Rayner, P., , and Scholze, M.: Towards a European operational observing system to monitor fossil CO2 emissions, Final report from the expert group, European Comission, Tech. rep., European Comission, 2015.

Conley, S., Franco, G., Faloona, I., Blake, D. R., Peischl, J., and Ryerson, T. B.: Methane emissions from the 2015 Aliso Canyon blowout in Los Angeles, CA, Science, 351, 1317–1320, doi:10.1126/science.aaf2348, 2016.

Dennison, P. E., Thorpe, A. K., Pardyjak, E. R., Roberts, D. A., Qi, Y., Green, R. O., Bradley, E. S., and Funk, C. C.: High spatial resolution mapping of elevated atmospheric carbon dioxide using airborne imaging spectroscopy: Radiative transfer modeling and power plant plume detection, Remote Sensing of Environment, 139, 116–129, doi:10.1016/j.rse.2013.08.001, 2013.

Deschamps, A., Marion, R., Briottet, X., Foucher, P., and Lavigne, C.: Simultaneous CO2 and aerosol retrieval in a vegetation fire plume using AVIRIS hyperspectral data, doi:10.1109/WHISPERS.2011.6080896, 2011.

EIA: U.S. Energy Information Administraton, EIA annual energy outlook 2013, Tech. rep., U.S. Energy Information Administraton, 2013.

EIA: U.S. Energy Information Administraton, Top 100 U.S. oil and gas fields, Tech. rep., U.S. Energy Information Administraton, 2015.

EPA: U.S. Environmental Protection Agency, Inventory of U.S. Greenhouse Gas Emissions and Sinks: 1990–2014, Technical Report EPA 430-R-16-002 (Environmental Protection Agency), Tech. rep., U.S. Environmental Protection Agency, 2016a.

EPA: U.S. Environmental Protection Agency, 2015 Greenhouse Gas Emissions from Large Facilities, https://ghgdata.epa.gov/, Tech. rep., U.S. Environmental Protection Agency, 2016b.

Frankenberg, C., Platt, U., and Wagner, T.: Iterative maximum a posteriori (IMAP)-DOAS for retrieval of strongly absorbing trace gases: Model studies for CH4 and CO2 retrieval from near infrared spectra of SCIAMACHY onboard ENVISAT, Atmospheric Chemistry and Physics, 5, 9–22, doi:10.5194/acp-5-9-2005, 2005.

Frankenberg, C., Thorpe, A. K., Thompson, D. R., Hulley, G., Kort, E. A., Vance, N., Borchardt, J., Krings, T., Gerilowski, K., Sweeney, C., Conley, S., Bue, B. D., Aubrey, A. D., Hook, S., and Green, R. O.: Airborne methane remote measurements reveal heavy-tail flux distribution in Four Corners region, Proceedings of the National Academy of Sciences of the United States of America, 113, 9734–9739, doi:10.1073/pnas.1605617113, 2016.

Galfalk, M., Olofsson, G., Crill, P., and Bastviken, D.: Making methane visible, Nature Climate Change, 6, 426–430, doi:10.1038/nclimate2877, 2016.

Gao, B. C. and Goetz, A. F. H.: Column atmospheric water-vapor and vegetation liquid water retrievals from airborne imaging spectrometer data, Journal of Geophysical Research-Atmospheres, 95, 3549–3564, doi:10.1029/JD095iD04p03549, 1990.

Gerilowski, K., Tretner, A., Krings, T., Buchwitz, M., Bertagnolio, P. P., Belemezov, F., Erzinger, J., Burrows, J. P., and Bovensmann, H.: MAMAP - a new spectrometer system for column-averaged methane and carbon dioxide observations from aircraft: instrument description and performance analysis, Atmospheric Measurement Techniques, 4, 215–243, doi:10.5194/amt-4-215-2011, 2011.

Green, R. O., Eastwood, M. L., Sarture, C. M., Chrien, T. G., Aronsson, M., Chippendale, B. J., Faust, J. A., Pavri, B. E., Chovit, C. J., Solis, M. S., Olah, M. R., and Williams, O.: Imaging spectroscopy and the Airborne Visible Infrared Imaging Spectrometer (AVIRIS), Remote Sensing of Environment, 65, 227–248, doi:10.1016/S0034-4257(98)00064-9, 1998.

Hamlin, L., Green, R., Mouroulis, P., Eastwood, M., Wilson, D., Dudik, M., and Paine, C.: Imaging spectrometer science measurements for terrestrial ecology: AVIRIS and new developments, doi:10.1109/AERO.2011.5747395, 2011.

Hopkins, F. M., Kort, E. A., Bush, S. E., Ehleringer, J. R., Lai, C. T., Blake, D. R., and Randerson, J. T.: Spatial patterns and source attribution of urban methane in the Los Angeles Basin, Journal of Geophysical Research-Atmospheres, 121, 2490–2507, doi:10.1002/2015JD024429, 2016.

Hulley, G. C., Duren, R. M., Hopkins, F. M., Hook, S. J., Vance, N., Guillevic, P., Johnson, W. R., Eng, B. T., Mihaly, J. M., Jovanovic, V. M., Chazanoff, S. L., Staniszewski, Z. K., Kuai, L., Worden, J., Frankenberg, C., Rivera, G., Aubrey, A. D., Miller, C. E., Malakar, N. K., Tomas, J. M. S., and Holmes, K. T.: High spatial resolution imaging of methane and other trace gases with the airborne Hyperspectral Thermal Emission Spectrometer (HyTES), Atmospheric Measurement Techniques, 9, 2393–2408, doi:10.5194/amt-9-2393-2016, 2016.

Jackson, R. B., Down, A., Phillips, N. G., Ackley, R. C., Cook, C. W., Plata, D. L., and Zhao, K. G.: Natural gas pipeline leaks across Washington, DC, Environmental Science and Technology, 48, 2051–2058, doi:10.1021/es404474x, 2014.

Johnson, D. R., Covington, A. N., and Clark, N. N.: Methane Emissions from leak and loss audits of natural gas compressor stations and storage facilities, Environmental Science and Technology, 49, 8132–8138, doi:10.1021/es506163m, 2015.

Kalnay, E., Kanamitsu, M., Kistler, R., Collins, W., Deaven, D., Gandin, L., Iredell, M., Saha, S., White, G., Woollen, J., Zhu, Y., Chelliah, M., Ebisuzaki, W., Higgins, W., Janowiak, J., Mo, K. C., Ropelewski, C., Wang, J., Leetmaa, A., Reynolds, R., Jenne, R., and Joseph, D.: The NCEP/NCAR 40-year reanalysis project, Bulletin of the American Meteorological Society, 77, 437–471, doi:10.1175/1520-0477(1996)077<0437:TNYRP>2.0.CO;2, 1996.

Karion, A., Sweeney, C., Petron, G., Frost, G., Hardesty, R. M., Kofler, J., Miller, B. R., Newberger, T., Wolter, S., Banta, R., Brewer, A., Dlugokencky, E., Lang, P., Montzka, S. A., Schnell, R., Tans, P., Trainer, M., Zamora, R., and Conley, S.: Methane emissions estimate from airborne measurements over a western United States natural gas field, Geophysical Research Letters, 40, 4393–4397, doi:10.1002/grl.50811, 2013.

Kirschke, S., Bousquet, P., Ciais, P., Saunois, M., Canadell, J. G., Dlugokencky, E. J., Bergamaschi, P., Bergmann, D., Blake, D. R., Bruhwiler, L., Cameron-Smith, P., Castaldi, S., Chevallier, F., Feng, L., Fraser, A., Heimann, M., Hodson, E. L., Houweling, S., Josse, B., Fraser, P. J., Krummel, P. B., Lamarque, J. F., Langenfelds, R. L., Le Quere, C., Naik, V., O'Doherty, S., Palmer, P. I., Pison, I., Plummer, D., Poulter, B., Prinn, R. G., Rigby, M., Ringeval, B., Santini, M., Schmidt, M., Shindell, D. T., Simpson, I. J., Spahni, R., Steele, L. P., Strode, S. A., Sudo, K., Szopa, S., van der Werf, G. R., Voulgarakis, A., van Weele, M., Weiss, R. F., Williams, J. E., and Zeng, G.: Three decades of global methane sources and sinks, Nature Geoscience, 6, 813–823, doi:10.1038/ngeo1955, 2013.

Kneizys, F. X., Abreu, L. W., Anderson, G. P., Chetwynd, J. H., Shettle, E. P., Robertson, D. C., Acharya, P., Rothman, L., Selby, J. E. A., Gallery, W. O., and Clough, S. A.: The MODTRAN 2/3 report and LOWTRAN 7 model, Tech. rep., Tech. rep., Phillips Laboratory, Geophysics Directorate, 1996.

Kort, E. A., Frankenberg, C., Costigan, K. R., Lindenmaier, R., Dubey, M. K., and Wunch, D.: Four Corners: The largest US methane anomaly viewed from space, Geophysical Research Letters, p. 2014GL061503, doi:10.1002/2014GL061503, 2014.

Krautwurst, S., Gerilowski, K., Jonsson, H. H., Thompson, D. R., Kolyer, R. W., Thorpe, A. K., Horstjann, M., Eastwood, M., Leifer, I., Vigil, S., Krings, T., Borchardt, J., Buchwitz, M., Fladeland, M. M., Burrows, J. P., and Bovensmann, H.: Methane emissions from a California landfill, determined from airborne remote sensing and in-situ measurements, Atmospheric Measurement Techniques Discussions, doi:10.5194/amt-2016-391, 2016.

Krings, T., Gerilowski, K., Buchwitz, M., Reuter, M., Tretner, A., Erzinger, J., Heinze, D., Pfluger, U., Burrows, J. P., and Bovensmann, H.: MAMAP – a new spectrometer system for column-averaged methane and carbon dioxide observations from aircraft: retrieval algorithm and first inversions for point source emission rates, Atmospheric Measurement Techniques, 4, 1735–1758, doi:10.5194/amt-4-1735-2011, 2011.

Krings, T., Gerilowski, K., Buchwitz, M., Hartmann, J., Sachs, T., Erzinger, J., Burrows, J. P., and Bovensmann, H.: Quantification of methane emission rates from coal mine ventilation shafts using airborne remote sensing data, Atmospheric Measurement Techniques, 6, 151–166, doi:10.5194/amt-6-151-2013, 2013.

Kuai, L., Worden, J. R., Li, K. F., Hulley, G. C., Hopkins, F. M., Miller, C. E., Hook, S. J., Duren, R. M., and Aubrey, A. D.: Characterization of anthropogenic methane plumes with the Hyperspectral Thermal Emission Spectrometer (HyTES): A retrieval method and error analysis, Atmospheric Measurement Techniques, 9, 3165–3173, doi:10.5194/amt-9-3165-2016, 2016.

Lavoie, T. N., Shepson, P. B., Cambaliza, M. O. L., Stirm, B. H., Karion, A., Sweeney, C., Yacovitch, T. I., Herndon, S. C., Lan, X., and Lyon, D.: Aircraft-based measurements of point source methane emissions in the Barnett Shale Basin, Environmental Science & Technology, 49, 7904–7913, doi:10.1021/acs.est.5b00410, 2015.

LTE: 2015 Fruitland outcrop monitoring report ,La Plata County, Colorado, Tech. rep., LT Environmental, Inc., http://cogcc.state.co.us/documents/library/AreaReports/SanJuanBasin/3m_project/2015%20FRUITLAND%20OUTCROP%20MONITORING%20REPORT_La_Plata.pdf, 2015.

Lyon, D. R., Zavala-Araiza, D., Alvarez, R. A., Harriss, R., Palacios, V., Lan, X., Talbot, R., Lavoie, T., Shepson, P., Yacovitch, T. I., Herndon, S. C., Marchese, A. J., Zimmerle, D., Robinson, A. L., and Hamburg, S. P.: Constructing a Spatially Resolved Methane Emission Inventory for the Barnett Shale Region, Environmental Science & Technology, 49, 8147–8157, doi:10.1021/es506359c, 2015.

Marion, R., Michel, W., and Faye, C.: Measuring trace gases in plumes from hyperspectral remotely sensed data, Ieee Transactions on Geoscience and Remote Sensing, 42, 854–864, doi:10.1109/TGRS.2003.820604, 2004.

Miller, S., Wofsy, S., Michalak, A., Kort, E. A., Andrews, A., Biraud, S., Dlugockenky, E. J., Eluszkiewicz, J., Fisher, M., Janssens-Maenhout, G., Miller, B., Miller, J., Montzka, S., Nehrkorn, T., and Sweeney, C.: Anthropogenic emissions of methane in the United States, Proceedings of the National Academy of Sciences of the United States of America, 110, doi:10.1073/pnas.1314392110, 2013.

Myhre, G., Shindell, D., Bréon, F.-M., Collins, W., Fuglestvedt, J., Huang, J., Koch, D., Lamarque, J., Lee, D., Mendoza, B., Nakajima, T., Robock, A., Stephens, G., Takemura, T., and Zhang, H.: Anthropogenic and natural radiative forcing. In: Climate change 2013: The physical science basis. Contribution of Working Group I to the Fifth Assessment Report of the Intergovernmental Panel on Climate Change, Tech. rep., Intergovernmental Panel on Climate Change, 2013.

Nisbet, E. G., Dlugokencky, E. J., and Bousquet, P.: Methane on the rise—again, Science, 343, 493–495, doi:10.1126/science.1247828, 2014.

NOAA: GMD measurement locations, National Oceanic & Atmospheric Administration (NOAA), Earth System Research Laboratory, Global Monitoring Division, Tech. rep., National Oceanic & Atmospheric Administration, 2015.

NRC: National Research Council committee on methods for estimating greenhouse gas emissions; Verifying greenhouse gas emissions: Methods to support international climate agreements, The National Academies Press, Washington, D.C., 2010.

Ogunjemiyo, S., Roberts, D. A., Keightley, K., Ustin, S. L., Hinckley, T., and Lamb, B.: Evaluating the relationship between AVIRIS water vapor and poplar plantation evapotranspiration, Journal of Geophysical Research, 107, doi:10.1029/2001JD001194, 2004.

Phillips, N. G., Ackley, R., Crosson, E. R., Down, A., Hutyra, L. R., Brondfield, M., Karr, J. D., Zhao, K. G., and Jackson, R. B.: Mapping urban pipeline leaks: Methane leaks across Boston, Environmental Pollution, 173, 1–4, doi:10.1016/j.envpol.2012.11.003, 2013.

Rella, C. W., Tsai, T. R., Botkin, C. G., Crosson, E. R., and Steele, D.: Measuring emissions from oil and natural gas well pads using the mobile flux plane technique, Environmental Science & Technology, 49, 4742–4748, doi:10.1021/acs.est.5b00099, 2015.

Roberts, D. A., Bradley, E. S., Cheung, R., Leifer, I., Dennison, P. E., and Margolis, J. S.: Mapping methane emissions from a marine geological seep source using imaging spectrometry, Remote Sensing of Environment, 114, 592–606, doi:10.1016/j.rse.2009.10.015, 2010.

Rodgers, C. D.: Inverse methods for atmospheric sounding, theory and practice, World Scientific, London, 2000.

Rothman, L. S., Gordon, I. E., Barbe, A., Benner, D. C., Bernath, P. E., Birk, M., Boudon, V., Brown, L. R., Campargue, A., Champion, J. P., Chance, K., Coudert, L. H., Dana, V., Devi, V. M., Fally, S., Flaud, J. M., Gamache, R. R., Goldman, A., Jacquemart, D., Kleiner, I., Lacome, N., Lafferty, W. J., Mandin, J. Y., Massie, S. T., Mikhailenko, S. N., Miller, C. E., Moazzen-Ahmadi, N., Naumenko, O. V., Nikitin, A. V., Orphal, J., Perevalov, V. I., Perrin, A., Predoi-Cross, A., Rinsland, C. P., Rotger, M., Simeckova, M., Smith, M. A. H., Sung, K., Tashkun, S. A., Tennyson, J., Toth, R. A., Vandaele, A. C., and Vander Auwera, J.: The HITRAN 2008 molecular spectroscopic database, Journal of Quantitative Spectroscopy & Radiative Transfer, 110, 533–572, doi:10.1016/j.jqsrt.2009.02.013, 2009.

Schaefer, H., Mikaloff Fletcher, S. E., Veidt, C., Lassey, K. R., Brailsford, G. W., Bromley, T. M., Dlugokencky, E. J., Michel, S. E., Miller, J. B., Levin, I., Lowe, D. C., Martin, R. J., Vaughn, B. H., and White, J. W. C.: A 21st century shift from fossil-fuel to biogenic methane emissions indicated by 13CH4, Science, doi:10.1126/science.aad2705, 2016.

Schwietzke, S., Sherwood, O. A., Bruhwiler, L. M. P., Miller, J. B., Etiope, G., Dlugokencky, E. J., Michel, S. E., Arling, V. A., Vaughn, B. H., White, J. W. C., and Tans, P. P.: Upward revision of global fossil fuel methane emissions based on isotope database, Nature, 538, doi:10.1038/nature19797, 2016.

Smith, M. L., Kort, E. A., Karion, A., Sweeney, C., Herndon, S. C., and Yacovitch, T. I.: Airborne ethane observations in the Barnett Shale: Quantification of ethane flux and attribution of methane emissions, Environmental Science & Technology, 49, 8158–8166, doi:10.1021/acs.est.5b00219, 2015.

Thompson, D. R., Gao, B. C., Green, R. O., Dennison, P. E., Roberts, D. A., and Lundeen, S.: Atmospheric Correction for Global Mapping Spectroscopy: Advances for the HyspIRI Preparatory Campaign, Remote Sensing of Environment, 167, 64–77, doi:10.1016/j.rse.2015.02.010, 2015a.

Thompson, D. R., Leifer, I., Bovensmann, H., Eastwood, M., Fladeland, M., Frankenberg, C., Gerilowski, K., Green, R. O., Kratwurst, S., Krings, T., Luna, B., and Thorpe, A. K.: Real-time remote detection and measurement for airborne imaging spectroscopy: a case study with methane, Atmospheric Measurement Techniques, 8, 4383–4397, doi:10.5194/amt-8-4383-2015, 2015b.

Thompson, D. R., Thorpe, A. K., Frankenberg, C., Green, R. O., Duren, R., Guanter, L., Hollstein, A., Middleton, E., Ong, L., and Ungar, S.: Space-based remote imaging spectroscopy of the Aliso Canyon CH4 superemitter, Geophysical Research Letters, 43, 6571–6578, doi:10.1002/2016GL069079, 2016.

Thorpe, A., Frankenberg, C., and Roberts, D.: Retrieval techniques for airborne imaging of methane concentrations using high spatial and moderate spectral resolution: Application to AVIRIS, Atmospheric Measurement Techniques, 7, 491–506, doi:10.5194/amt-7-491-2014, 2014.

Thorpe, A. K., Frankenberg, C., Aubrey, A. D., Roberts, D. A., Nottrott, A. A., Rahn, T. A., Sauer, J. A., Dubey, M. K., Costigan, K. R., Arata, C., Steffke, A. M., Hills, S., Haselwimmer, C., Charlesworth, D., Funk, C. C., Green, R. O., Lundeen, S. R., Boardman, J. W., Eastwood, M. L., Sarture, C. M., Nolte, S. H., Mccubbin, I. B., Thompson, D. R., and McFadden, J. P.: Mapping methane concentrations from a controlled release experiment using the next generation airborne visible/infrared imaging spectrometer (AVIRIS-NG), Remote Sensing of Environment, 179, 104–115, doi:10.1016/j.rse.2016.03.032, 2016a.

Thorpe, A. K., Frankenberg, C., Green, R. O., Thompson, D. R., Aubrey, A. D., Mouroulis, P., Eastwood, M. L., and Matheou, G.: The Airborne Methane Plume Spectrometer (AMPS): Quantitative imaging of methane plumes in real time, 2016 IEEE Aerospace Conference, doi:10.1109/AERO.2016.7500756, 2016b.

Tratt, D. M., Buckland, K. N., Hall, J. L., Johnson, P. D., Keim, E. R., Leifer, I., Westberg, K., and Young, S. J.: Airborne visualization and quantification of discrete methane sources in the environment, Remote Sensing of Environment, 154, 74–88, doi:10.1016/j.rse.2014.08.011, 2014.

TRI: Tri-State Generation and Transmission Association, http://www.tsgt.coop/AboutUs/baseload-resources.cfm, Tech. rep., Tri-State Generation and Transmission Association, 2016.

Turner, A. J., Jacob, D. J., Wecht, K. J., Maasakkers, J. D., Lundgren, E., Andrews, A. E., Biraud, S. C., Boesch, H., Bowman, K. W., Deutscher, N. M., Dubey, M. K., Griffith, D. W. T., Hase, F., Kuze, A., Notholt, J., Ohyama, H., Parker, R., Payne, V. H., Sussmann, R., Sweeney, C., Velazco, V. A., Warneke, T., Wennberg, P. O., and Wunch, D.: Estimating global and North American methane emissions with high spatial resolution using GOSAT satellite data, Atmospheric Chemistry and Physics, 15, 7049–7069, doi:10.5194/acp-15-7049-2015, 2015.

Wecht, K. J., Jacob, D. J., Frankenberg, C., Jiang, Z., and Blake, D. R.: Mapping of North American methane emissions with high spatial resolution by inversion of SCIAMACHY satellite data, Journal of Geophysical Research-Atmospheres, 119, 7741–7756, doi:10.1002/2014JD021551, 2014.

Williams: NASA study shows one detection of methane in multiple surveys of Ignacio plant, Tech. rep., Williams Partners L.P., https://blog.williams.com/projects-and-operations/nasa-study-shows-no-detection-of-methane-in-multiple-surveys-of-ignacio-plant/, 2016.

Zavala-Araiza, D., Lyon, D., Alvarez, R. A., Palacios, V., Harriss, R., Lan, X., Talbot, R., and Hamburg, S. P.: Toward a functional definition of methane super-emitters: Application to natural gas production sites, Environmental Science & Technology, 49, 8167–8174, doi:10.1021/acs.est.5b00133, 2015.